ROBUST NONLINEAR CONTROL AND ESTIMATION OF AN PRRR ROBOT SYSTEM

Mohammad AlShabi[1*], Khaled S. Hatamleh[2], S. Andrew Gadsden[3], and Bassel Soudan[4]

Abstract – In this paper, a newly proposed implementation of an unscented smooth variable structure filter (UK-SVSF) is introduced. The method is combined with a sliding mode controller (SMC) to compensate for modeling uncertainties. The robustness and tracking accuracy of the proposed controller and estimation strategy are demonstrated on a four degree-of-freedom (DOF) robotic system with one prismatic and three rotary joints (PRRR). The effectiveness of the proposed combination is proven through comparisons with three types of nonlinear estimation strategies: the standard unscented Kalman filter (UKF), smooth variable structure filter (SVSF), and a previously published UK-SVSF. The robot's trajectory following accuracy and efficiency are used as the performance parameters to study and compare the different strategies. Modeling uncertainties are added to the system to provide a more thorough evaluation of the robustness of the different nonlinear control and estimation strategies.

***Keywords*—Sliding Mode Controller; Unscented Kalman Filter; Smooth Variable Structure Filter; Estimation; Modeling Uncertainties.**

1. INTRODUCTION

The field of robotics is rapidly expanding into major aspects of modern life. Robotic arms are becoming commonplace in surgical theaters and space exploration, in prosthetics and life enhancement for the handicapped, as surrogates in dangerous military and safety operations, and most prevalently for repetitive high-precision industrial and manufacturing tasks. This has necessitated the development of control strategies that guarantee efficient, and more importantly, precisely accurate maneuverability of the robotics. Researchers have been working on control methods that enable a robot to follow a desired trajectory while minimizing the effects of external disturbances and modeling uncertainties.

Versatile robots typically have multiple joints with multiple degrees of freedom. Because of this, they are classified as a multi-input, multi-output (MIMO) control problem. Due to the nonlinearities involved, linear control methods such as Proportional-Integral (PI), Proportional-Derivative (PD), and PID are rarely employed for MIMO robotic arms [1, 2]. Researchers have demonstrated robust behavior utilizing nonlinear controllers based on Fuzzy-Logic [3-5]. Other researchers have proposed nonlinear sliding mode controllers (SMC). While these methods achieve robust control, the robustness comes at a cost of chattering or high frequency switching [1, 6-8]. Chattering

[1] [1]M. Al-Shabi is an Assistant Professor with the Mechanical Engineering Department in the College of Engineering at the University of Sharjah, Sharjah, United Arab Emirates, 27272 (malshabi@sharjah.ac.ae). * Corresponding Author.
[2]K. S. Hatamleh is an Assistant Professor with the Mechanical Engineering Department at Jordan University of Science and Technology, Irbid, Jordan, 22110 (kshh@just.edu.jo).
[3]S. A. Gadsden is an Assistant Professor of Mechanical Engineering with the College of Engineering and Physical Sciences at the University of Guelph, Ontario, Canada, N1G 2W1 (gadsden@uoguelph.ca).
[4]B. Soudan is an Associate Professor with the Department of Electrical and Computer Engineering at the University of Sharjah, Sharjah, United Arab Emirates, (bsoudan@sharjah.ac.ae).

becomes pronounced especially when there is significant noise in the feedback signals from the sensors. Bear in mind that modern controllers employ a very large number of sensors to achieve better perception of the environment. The numerous sensor inputs, and their unavoidable associated signal noise, multiply the problem many fold. Because of that, feedback signals are now typically processed to reduce the noise and improve the stability of the controller.

Estimation strategies have been proven instrumental in reducing the effect of noisy sensor measurements as well as in extracting non-measured state values at the same time. They have become common in the feedback of most controllers. In 1942, the Wiener Filter was introduced based on least square error method. It offered the first solution to dealing with stochastic noise [9-11]. Shortly after, the predictor-corrector Kalman Filter (KF) was introduced [9-13]. However, the Kalman Filter places strict restrictions on the estimation problem. The system needs to be known and linear, and the noise is assumed to be white and Gaussian. This is not necessarily the case in real-world systems, which causes the Kalman filter to fail in most practical applications. A number of extensions have been made on the KF in an effort to improve its robustness and stability for nonlinear systems. These adaptations include: the Extended Kalman Filter (EKF) [11, 14-16], the Iterated Extended Kalman Filter (IKF) [11-12, 17-19], the Higher-Order Extended Kalman Filter (HOEKF) [11, 20-22], the Sigma-Point Kalman Filter (SPKF) variations which include the Unscented Kalman Filter (UKF) [11, 23-27], the Particle Filter (PF) [28], Sliding Mode Observers [29-37], and the Smooth Variable Structure Filter (SVSF) [38-46]. The SVSF is an estimation technique that was developed in 2007 and is used to estimate linear and non-nonlinear systems. It exhibits high resistance to uncertainties, but it is prone to sensitivity to measurement noise. The sensitivity becomes problematic as noise amplitude increases. Several variations have been proposed to address this issue [38-46], including the Unscented Smooth Variable Structure Filter (UK-SVSF) [47-51]. The benefits of the combination are to be stable and robust against the uncertainties in the model using the SVSF's features, while reducing the noise sensitivity using the UKF's features.

In this work, we will introduce a new closed loop controller system that consists of a Sliding Mode Controller (SMC) combined with a newly proposed UK-SVSF as the feedback. The proposed method is considered stable, as per Appendix A3-2. The root mean square error will be significantly reduced compared with the original SVSF and the older version of the UK-SVSF in extreme cases (few measurements, high system and measurement noise amplitudes, and system modeling uncertainties). This proposed system will be evaluated using a four degree of freedom (DOF) robotic arm that has one planer and three rotary joints (PRRR). Matlab-Simulink simulations will be discussed to show the effect of noise on the performance of the filter and the overall control system. Section 2 of develops the mathematical derivations of the robotic arm's forward and inverse kinematic solutions, joint space trajectories, and overall dynamics. The implemented Sliding Mode Controller (SMC) is discussed in section 3, and then section 4 describes the proposed implementation of the UK-SVSF and discusses its advantages compared to three other nonlinear estimation strategies: Unscented Kalman Filter (UKF), Smooth Variable Structure Filter (SVSF), and the previously published Unscented Smooth Variable Structure Filter (UK-SVSF). Modeling uncertainty is added to the system to provide a more thorough comparison of control and estimation robustness and tracking accuracy. The results of applying the nonlinear controller and the four nonlinear estimation strategies are described in Sections 5 and 6, respectively. The paper is concluded and future work is discussed in Section 7.

2. Modeling the 4-DOF PRRR Robotic Arm Dynamics

As discussed in the previous section, we will use a 4-DOF PRRR robotic arm as the evaluation apparatus for the proposed control method as well as benchmarking with other control methods. Therefore, in this section, we will start by developing the mathematical model for the robotic arm's dynamics. Figure 1 shows a pictorial view of the robotic arm under consideration and the diagrams in Figure 2 through Figure 4 outline the frame and joint assignments. Common parameters are listed in Table 1 and were determined using the procedure defined in [52].

Table 1 –Denavit-Harternberg (D-H) parameters for PRRR reference frame [53-57].

Link	a_{i-1}	α_{i-1}	d_i	θ_i
1	0	0	d_1	0
2	a_1	0	0	θ_1
3	a_2	0	0	θ_2
4	a_3	0	0	θ_3
5	0	0	d_4	0

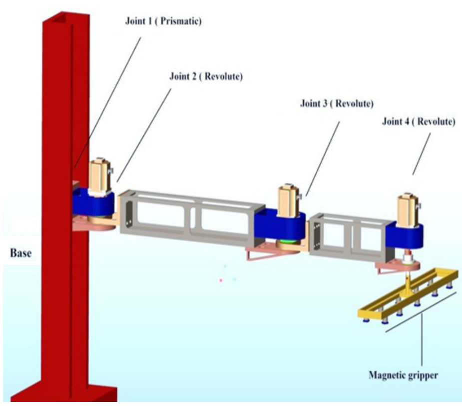

Figure 1 – Pictorial impression of the PRRR robotic arm used in this work [53-57].

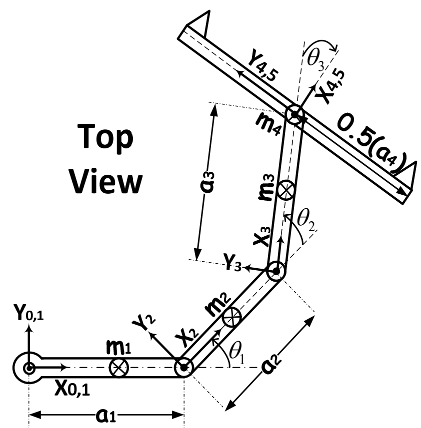

Figure 2 –Top view of PRRR robotic arm [53-57].

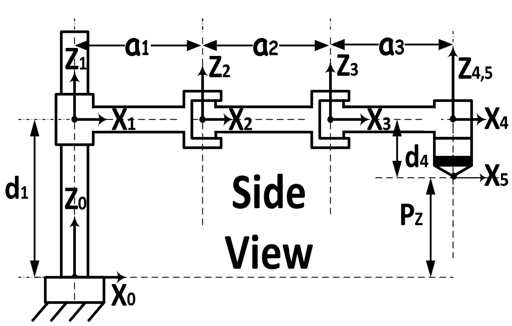

Figure 3 – Side view of PRRR robotic arm [53-57].

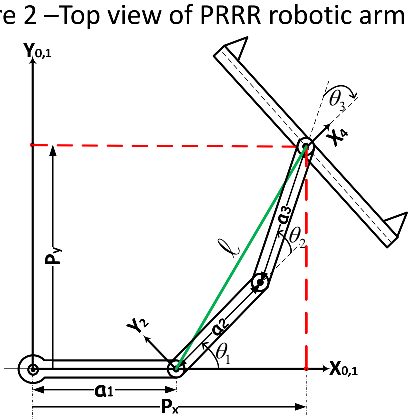

Figure 4 –Graphical solution of the inverse kinematics problem [53-57].

2.1. Forward Kinematic Solution

The forward kinematic solution provides dynamic equations that can be used to model and study the 4-DOF robotic arm. The solution is obtained using a transformation matrix ${}^{0}_{5}\mathbf{T}$ that provides the orientation and position of the end effector (arm) with respect to the base (or zero) frame. Equation 1 below shows the forward kinematic solution for our system where a subscript defines the reference frame's number, while the superscript defines the frame in which the orientation is needed.

$$
{}^{0}_{5}\mathbf{T} = {}^{0}_{1}\mathbf{T}\,{}^{1}_{2}\mathbf{T}\,{}^{2}_{3}\mathbf{T}\,{}^{3}_{4}\mathbf{T}\,{}^{4}_{5}\mathbf{T} = \begin{bmatrix} c_{123} & -s_{123} & 0 & (a_1 + a_2 c_1 + a_3 c_{12}) \\ s_{123} & c_{123} & 0 & (a_2 s_1 + a_3 s_{12}) \\ 0 & 0 & 1 & (d_1 + d_4) \\ 0 & 0 & 0 & 1 \end{bmatrix} \tag{1}
$$

2.2. Inverse Kinematic Solution

Suppose that the known transformation matrix ${}^{0}_{5}\mathbf{T}_d$, shown in equation 2 below, describes the desired position and orientation of the end effector. Using this matrix, we need to develop relationships to obtain appropriate values for the four parameters required to maneuver the arm correctly (d_1, θ_1, θ_2, θ_3). Based on the robot diagram shown in Figure 4 we can calculate the graphical inverse kinematic equations as shown in equations 3 through 10 below [53-57].

$$
{}^{0}_{5}\mathbf{T}_d = \begin{bmatrix} r_{11} & r_{12} & r_{13} & P_x \\ r_{21} & r_{22} & r_{23} & P_y \\ r_{31} & r_{32} & r_{33} & P_z \\ 0 & 0 & 0 & 1 \end{bmatrix} \tag{2}
$$

First, we can apply Pythagoras theorem to the right triangle made up of $\ell, (P_x - a_1)$ and P_y, to obtain a relationship between extension ℓ and link length a_1 and the position components P_x and P_y:

$$
\ell^2 = (P_x - a_1)^2 + P_y^2 \tag{3}
$$

We can also develop a relationship between extension ℓ and link lengths a_2 and a_3 using the Cosine law:

$$
\ell^2 = a_2^2 + a_3^2 + 2a_2 a_3 c_2 \rightarrow c_2 = \frac{\ell^2 - a_2^2 - a_3^2}{2a_2 a_3} \tag{4}
$$

s_2 (defined in the glossary) can be obtained using the trigonometry relationship $c_2^2 + s_2^2 = 1$:

$$
s_2 = \pm\sqrt{1 - c_2^2} \tag{5}
$$

Using equations (4) and (5), θ_2 can be obtained as:

$$
\theta_2 = Atan2(s_2, c_2) \tag{6}
$$

Graphically it is possible to determine that $P_y = (a_3 c_2 + a_2)s_1 + a_3 s_2 c_1$ and $(P_x - a_1) = -a_3 s_2 s_1 + (a_3 c_2 + a_2)c_1$. Based on these values, s_1 and c_1 can be obtained as follows:

$$
P_y = (a_3 c_2 + a_2)s_1 + a_3 s_2 c_1 = k_1 s_1 + k_2 c_1 \tag{7}
$$

$$P_x - a_1 = -a_3 s_2 s_1 + (a_3 c_2 + a_2) c_1 = -k_2 s_1 + k_1 c_1$$

$$\begin{bmatrix} k_1 & k_2 \\ -k_2 & k_1 \end{bmatrix} \begin{bmatrix} s_1 \\ c_1 \end{bmatrix} = \begin{bmatrix} P_y \\ P_x - a_1 \end{bmatrix} \rightarrow \begin{bmatrix} s_1 \\ c_1 \end{bmatrix} = \begin{bmatrix} k_1 & k_2 \\ -k_2 & k_1 \end{bmatrix}^{-1} \begin{bmatrix} P_y \\ P_x - a_1 \end{bmatrix}$$

θ_1 is then obtained as:

$$\theta_1 = Atan2(s_1, c_1) \tag{8}$$

θ_3 can be obtained analytically by comparing equations (1) and (2), which yields:

$$\theta_1 + \theta_2 + \theta_3 = Atan2(r_{21}, r_{11}) \rightarrow \theta_3 = Atan2(r_{21}, r_{11}) - \theta_1 - \theta_2 \tag{9}$$

The remaining variable d_1 can be obtained graphically from Figure 4 or analytically by comparing equations (1) and (2), which will result in the following:

$$d_1 = P_z - d_4 \tag{10}$$

2.3. Joint Space Trajectory Generation

Suppose that the robot arm is used for picking and placing objects. The robot arm picks up products from a well-defined initial position and orientation that must be defined by an initial transformation matrix ${}^{0}_{5}\mathbf{T}_{initial}$. The robot then drops the product at another desired position and orientation described by the final transformation matrix ${}^{0}_{5}\mathbf{T}_{final}$. These two transformation matrices may be used to calculate the vector of initial joint space variables $\mathbf{\Theta}_{initial}$ and the vector of final joint space variables $\mathbf{\Theta}_{final}$. From the inverse kinematics solution derived above, we define the joint space variable vectors as follows:

$\mathbf{\Theta}_{initial} = \begin{bmatrix} d_{1,0} & \theta_{1,0} & \theta_{2,0} & \theta_{3,0} \end{bmatrix}^T$ and $\mathbf{\Theta}_{final} = \begin{bmatrix} d_{1,f} & \theta_{1,f} & \theta_{2,f} & \theta_{3,f} \end{bmatrix}^T$

It is assumed that the manipulator moves according to the following sequence:

- First, link 1 extends to reach the length d_1. Other joints are kept stationary during this motion to ensure that the arm will not hit other surrounding boxes.
- Once link 1 reaches length d_1, it will be held stationary at that position while the other three joints rotate with angles θ_1, θ_2 and θ_3, simultaneously.
- Once the desired angles are obtained, the motors are turned off, and the arm starts to descend to reach height P_z. Finally, the arm drops the box.
- The arm retracts following a similar sequence.

In order to describe the trajectory of each joint over a required operating time, the stationary periods will be assumed constant functions, while third-degree polynomials are generated to describe the movements for each joint. However, to solve the proposed polynomials, four initial conditions are needed for each relation. The calculated initial and final values for each joint provide two of the four conditions. The remaining conditions may be obtained by assuming zero initial and final velocities. As a result, a total of four functions consisting of polynomials and constants are obtained, refer to Figure 5. The four functions are referred to as $d_1(t)$, $\theta_1(t)$, $\theta_2(t)$

, and $\theta_3(t)$. These functions represent the desired joint space trajectories that a controller should follow in order to successfully pick-and-place an object with the robot. The controller needs to determine the required torque vectors for the robot joint motors, which can be calculated using dynamic models for the PRRR robot.

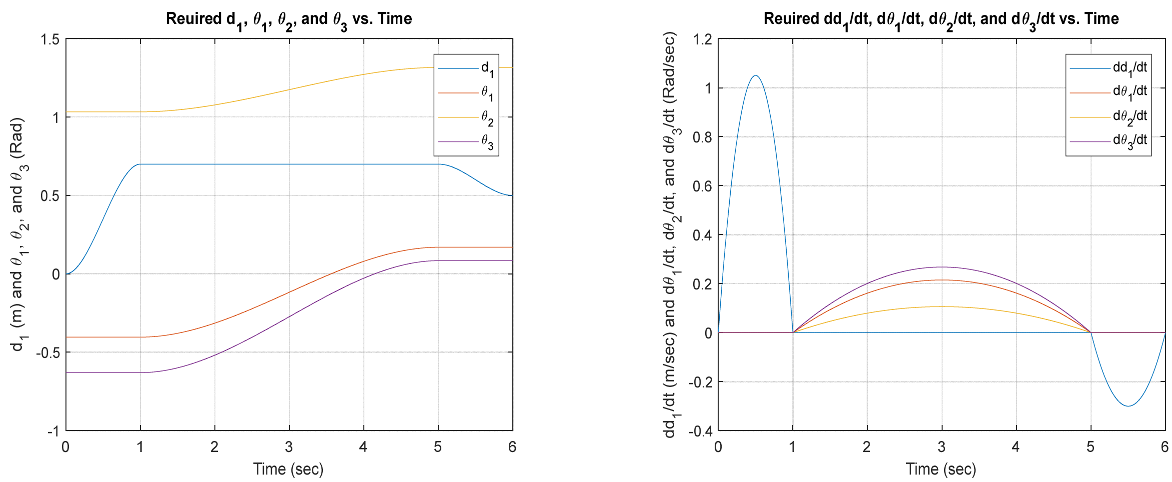

(a) (b)

Figure 5 – Desired prismatic and revolute joint trajectories over time.

2.4. Dynamics of the Robotic Arm

Assuming L is the total energy as defined in equation (11) below, and using the Lagrange-Euler relationship in equation (12), the PRRR dynamic behavior can be represented by the relationship in equation (13) [52]. Based on that, equations (14) through (16) describe the derivation of the equation of motion for the proposed manipulator.

$$L = \sum(Kinetic - Potential) = \sum\left(\frac{1}{2} m_i \, {}^{0}_{c_i}v^T \, {}^{0}_{c_i}v + \frac{1}{2} \, {}^{0}_{c_i}\omega^T I_i \, {}^{0}_{c_i}\omega + m_i \mathbf{g}^{0^T} \, {}^{0}_{c_i}r\right) \text{ where } \mathbf{g}^0 = \begin{bmatrix} 0 \\ 0 \\ -g \end{bmatrix} \tag{11}$$

$$\tau_i = \frac{d}{dt}\left(\frac{\partial L}{\partial \dot{\Theta}_i}\right) - \left(\frac{\partial L}{\partial \Theta_i}\right) \tag{12}$$

$$\boldsymbol{\tau} = \mathbf{M}(\boldsymbol{\Theta})\ddot{\boldsymbol{\Theta}} + \mathbf{V}(\boldsymbol{\Theta}, \dot{\boldsymbol{\Theta}}) + \mathbf{G}(\boldsymbol{\Theta}) \tag{13}$$

$$\begin{bmatrix} F \\ \tau_1 \\ \tau_2 \\ \tau_3 \end{bmatrix} = \begin{bmatrix} m_T & 0 & 0 & 0 \\ 0 & A_1 & A_4 & A_5 \\ 0 & A_4 & A_2 & A_6 \\ 0 & A_5 & A_6 & A_3 \end{bmatrix} \begin{bmatrix} \ddot{d}_1 \\ \ddot{\theta}_1 \\ \ddot{\theta}_2 \\ \ddot{\theta}_3 \end{bmatrix} + \begin{bmatrix} 0 \\ A_7 \\ A_8 \\ 0 \end{bmatrix} + \begin{bmatrix} -g m_T \\ 0 \\ 0 \\ 0 \end{bmatrix} \tag{14}$$

For the Sliding Mode Control, equation (13) is rewritten to have the form of

$$\boldsymbol{\tau} = \mathbf{M}(\boldsymbol{\Theta})\ddot{\boldsymbol{\Theta}} + \mathbf{Vn}(\boldsymbol{\Theta}, \dot{\boldsymbol{\Theta}})\dot{\boldsymbol{\Theta}} + \mathbf{G}(\boldsymbol{\Theta}) \tag{15}$$

Where

$$\mathbf{Vn}(\boldsymbol{\Theta}, \dot{\boldsymbol{\Theta}}) = \begin{bmatrix} 0 & 0 & 0 & 0 \\ \mathrm{B}_1 & \mathrm{B}_2 & 0 & 0 \\ \mathrm{B}_3 & 0 & 0 & 0 \\ 0 & 0 & 0 & 0 \end{bmatrix} \tag{16}$$

2.5. Jacobian Matrix

If the joint space trajectories $(\mathbf{\Theta},\dot{\mathbf{\Theta}},\ddot{\mathbf{\Theta}})$ are known, then the Cartesian space trajectories $(\mathbf{X},\dot{\mathbf{X}},\ddot{\mathbf{X}})$ can be computed as per equations (17) and (18) below:

$$\mathbf{X} = \begin{bmatrix} a_1 + a_2c_1 + a_3c_{12} \\ a_2s_1 + a_3s_{12} \\ d_1 + d_4 \\ (\theta_1 + \theta_2 + \theta_3) \end{bmatrix} \tag{17}$$

$$\dot{\mathbf{X}} = \mathbf{J}(\Theta)\dot{\Theta} \rightarrow \mathbf{J}(\mathbf{\Theta}) = \begin{bmatrix} 0 & -(a_2s_1 + a_3s_{12}) & -a_3s_{12} & 0 \\ 0 & (a_2c_1 + a_3c_{12}) & a_3c_{12} & 0 \\ 1 & 0 & 0 & 0 \\ 0 & 1 & 1 & 1 \end{bmatrix} \tag{18}$$

3. Sliding Mode Control Methodology

Sliding Mode Control (SMC) is a well-known nonlinear control strategy based on Variable Structure Control (VSC) theory. Variable Structure Control, in turn, is based on a discontinuous input gain that switches back-and-forth across a state space trajectory. Similarly, SMC uses a discontinuous control gain (i.e., a switching function) that keeps the state trajectory within a switching hyper-plane [58-61]. Both SMC and VSC are robust to unmodelled uncertainties and disturbances. An early and relatively crude example of SMC was presented in [58]. In that study, a rudder was used to force a ship to follow a pre-described path that was a function of the rudder angle δ and the course angle ϕ. The SMC consisted of two phases: the reachability phase, where the system dynamics are forced towards the desired one; and the sliding phase, where the trajectory is maintained around the desired trajectory. The system had a stable response and was less sensitive to modeling uncertainties [58]. Note however that SMC has some drawbacks, which can be summarized as:

- Chattering – High frequency switching across the hyper-plane. It can reduce accuracy of trajectory following, and increases wear on mechanical components [58, 62]. Fortunately, it is possible to reduce the effect of chattering by using a saturation function that smooths the chattering signal.
- Hysteresis.
- Delays caused by the switching signal.

Figure 6 illustrates the SMC proposed for this work. The controller defines a hyper-plane that has the form of $\mathbf{S} = \mathbf{e} + \boldsymbol{\lambda}\dot{\mathbf{e}}$, where $\mathbf{e}$ is the error between actual and desired trajectories. Note that these values include angles and displacements, as well as their derivatives.

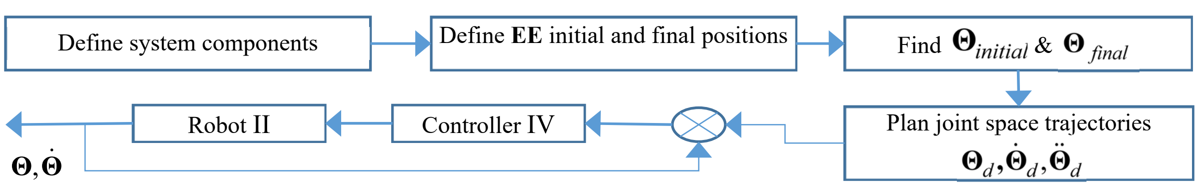

Figure 6 –A Schematic diagram for the proposed sliding mode controller [53-57].

The reachability phase uses the following gain:

$$\mathbf{u} = -\mathbf{M}(\mathbf{\Theta})\mathbf{K}\, sign(\mathbf{S}) \tag{19}$$

And, the sliding phase has an equivalent control signal that is derived by setting $\dot{\mathbf{S}} = \mathbf{0}$ as follows:

$$\mathbf{u}_{eq} = \mathbf{M}(\mathbf{\Theta})\left(\ddot{\mathbf{\Theta}}_{d} - \boldsymbol{\lambda}^{-1}\left(\dot{\mathbf{\Theta}} - \dot{\mathbf{\Theta}}_{\mathbf{d}}\right)\right) + \mathbf{Vn}\left(\mathbf{\Theta}, \dot{\mathbf{\Theta}}\right)\left(\dot{\mathbf{\Theta}}_{d} - \boldsymbol{\lambda}^{-1}\left(\mathbf{\Theta} - \mathbf{\Theta}_{\mathbf{d}}\right)\right) + \mathbf{G}(\mathbf{\Theta}) \tag{20}$$

Combining equations (19) and (20) creates the SMC input used by the PRRR system. Note that gain $\mathbf{K}$ must be large enough to compensate for uncertainties. However, it is important to note that chattering increases with higher $\mathbf{K}$ values. As such, the gain should be selected and designed carefully. Finally, note that the SMC response is found to be less sensitive to parameter changes; $\boldsymbol{\lambda}^{-1}$.

4. Estimation Methodologies

As it was mentioned earlier, estimation strategies have been proven instrumental in reducing the effect of noisy sensor measurements as well as in extracting non-measured state values at the same time. This section discusses a number of estimation methodologies and introduces our proposed UK-SVSF filter implementation.

4.1. Unscented Kalman Filter

The Kalman Filter (KF) has been shown as the optimal solution for linear and known systems with stochastic white noise. The KF was modified for nonlinear applications to the EKF, where the nonlinear functions are linearized to their corresponding Jacobian matrices [11]. Several other nonlinear methods have been developed, including: the Sigma-Point Kalman Filter (SPKF) family [11, 23-27] and the Particle Filter (PF) [28]. One of the varieties of SPKF is the Unscented Kalman Filter (UKF) chosen for this work. While the EKF utilizes a first-order Taylor series approximation, the UKF estimation strategy has been shown to be accurate up to the third-order [11]. The UKF defines sigma points that are drawn from the probability distribution function (PDF) projected for the states (as represented in Figure 7). These points are then propagated through the nonlinear model to obtain the a priori estimates. These values are combined together using tuned weight factors, and then they are refined to the a posteriori (or updated) estimates, which approximates the mean and covariance of the nonlinear distribution. The flowchart in Figure 8 summarizes the UKF estimation process. Note that:

$$\mathbf{P}_1 = \mathbf{P}_{k-1|k-1} \tag{21}$$

$$\mathbf{P}_2 = \mathbf{P}_{k|k-1} \tag{22}$$

$$\left(\boldsymbol{\varrho}_j\right)_i = \begin{cases} 0 & i = 0 \\ \left(\sqrt{n\mathbf{P}_j}\right)_i^T & 1 \le i \le n \\ -\left(\sqrt{n\mathbf{P}_j}\right)_i^T & n+1 \le i \le 2n \end{cases} \tag{23}$$

4.2. Smooth Variable Structure Filter

The Smooth Variable Structure Filter (SVSF) makes use of VSC theory and may be applied to both linear and nonlinear systems [38-46]. The flowchart in Figure 9 summarizes the SVSF estimation strategy algorithm. The SVSF utilizes a switching term that forces the state estimate to within a region of the true state trajectory, known as the existence subspace. Similar to the KF, the SVSF is formulated as a predictor-corrector, and has two indicators of performance assigned to each state [63, 64]. The predicted and updated existence subspaces are respectively defined as follows [63]:

$$\mathbf{e}_{x,k|k-1} = \mathbf{e}_{z,k|k-1} - \mathbf{v}_k \tag{24}$$
$$\mathbf{e}_{x,k|k} = \mathbf{e}_{z,k|k} - \mathbf{v}_k \tag{25}$$

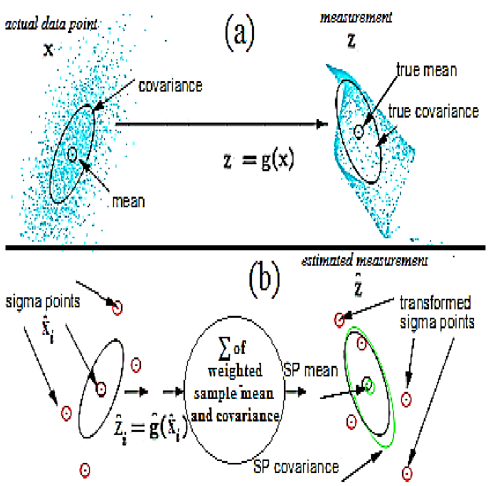

Figure 7 – (a) Actual system states and nonlinear measurements, and (b) the UKF's estimates [24, 25].

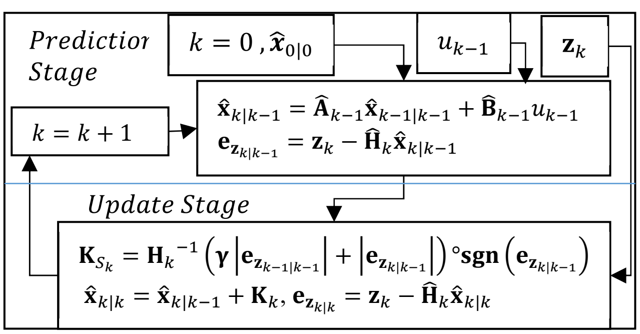

Figure 9 – The Smooth Variable Structure Filter algorithm [9, 64].

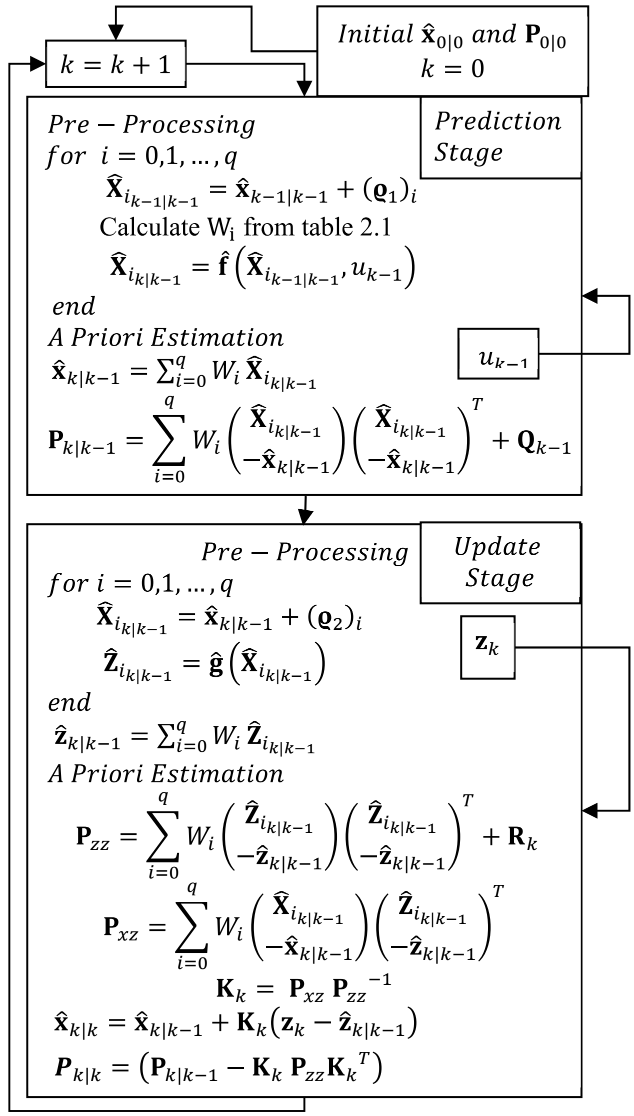

Figure 8 – The Unscented Kalman filter (UKF) estimation process [11, 63].

where both existence subspaces are functions of modeling uncertainties and noise signals. To minimize the effects of SVSF chattering, the sign function in the SVSF gain equation is replaced by a smoothing function. It is described by equation (26) with an appropriate smoothing boundary layer (SBL).

$$sat(e_{z_i,k|k-1}, \psi_i) = \begin{cases} e_{z_i,k|k-1}/\psi_i & e_{z_i,k|k-1} \le \psi_i \\ sign(e_{z_i,k|k-1}) & e_{z_i,k|k-1} > \psi_i \end{cases} \tag{26}$$

The SBL width should be chosen carefully. According to [64], large SBL values increase the estimation error, and may cause a slower convergence rate (refer to Figure 10 and Table 2). However, a small SBL width can lead to chattering and increased sensitivity to noise (as shown in Figure 11 and Table 3). If the control gain is not increased, then the system performance becomes unstable. The SBL value should be selected larger than the noise and modeling uncertainties.

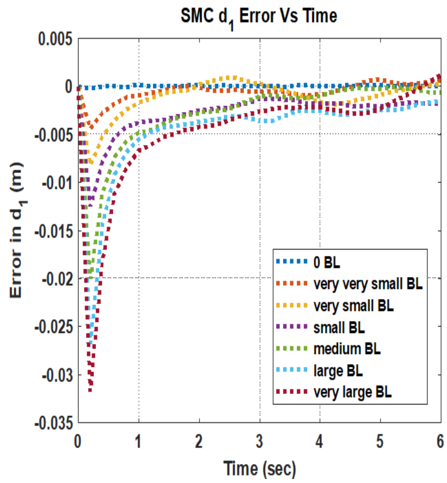

Figure 10 – The effect of the smooth boundary layer on the overall performance.

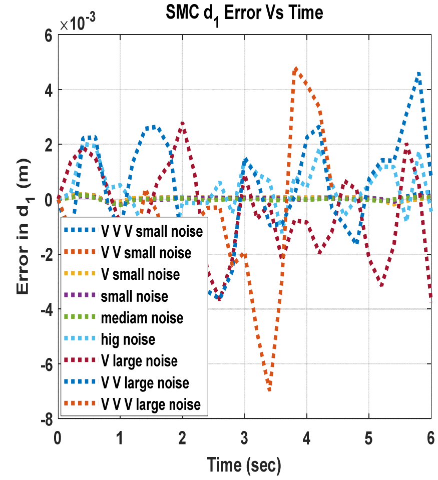

Figure 11 – The effect of measurement noise on the overall performance.

Table 2 – The root mean square error of the PRRR robot with different smooth boundary layers.

SBL	zero	v.v. small	v. small	small	medium	large	v. large
RMSE							
d (m)	0.00008	0.00123	0.00225	0.00374	0.00494	0.00652	0.00770
$\dot{d}$ (m/sec)	0.00451	0.00804	0.01294	0.01847	0.02649	0.03215	0.03640
θ_1 (rad)	0.00006	0.00201	0.00351	0.00566	0.00530	0.00706	0.00856
$\dot{\theta}_1$ (rad/sec)	0.00673	0.01512	0.02063	0.02311	0.02798	0.02894	0.03582
θ_2(rad)	0.00007	0.00246	0.00374	0.00667	0.00535	0.00671	0.00846
$\dot{\theta}_2$(rad/sec)	0.00680	0.02062	0.02665	0.02516	0.03397	0.03047	0.02811
θ_3(rad)	0.00006	0.00297	0.00489	0.00741	0.00762	0.01061	0.01184
$\dot{\theta}_3$(rad/sec)	0.00461	0.02738	0.03672	0.04134	0.04405	0.04057	0.04793

Table 3 – The root mean square error of the PRRR robot with different measurement noise amplitudes.

SBL	v.v.v. small	v.v. small	v. small	small	medium	large	v. large	v.v. large	v.v.v. large
RMSE	$\times 10^{-5}$	$\times 10^{-5}$	$\times 10^{-5}$	$\times 10^{-5}$	$\times 10^{-5}$	$\times 10^{-5}$	$\times 10^{-5}$	$\times 10^{-5}$	
d (m)	8.8	7.5	7.6	6.3	8.4	190	260	350	FAIL
$\dot{d}$ (m/sec)	540	540	440	500	510	1800	2300	3800	
θ_1 (rad)	11	16	16	10	12	300	370	310	
$\dot{\theta}_1$ (rad/sec)	820	830	840	860	840	3200	3600	4500	
θ_2(rad)	16	14	14	11	13	26	42	44	
$\dot{\theta}_2$(rad/sec)	820	840	930	870	860	2800	3500	4900	
θ_3(rad)	7.5	7.8	8.0	4.6	4.7	210	490	300	
$\dot{\theta}_3$(rad/sec)	460	450	460	490	460	1800	2200	3500	

4.3. The Unscented Smooth Variable Structure Filter

To improve the SVSF's performance, it was combined with the UKF (as in Figure 12) and is referred to as the UK-SVSF [65]. The algorithm in Figure 12 specifies that the UKF gain be used if no chattering occurs. However, if chattering is observed, the filter switches to the SVSF gain. Figure 13 illustrates the combined UK-SVSF estimation methodology [66]. Compared to both SVSF and UKF, the UK-SVSF estimation strategy offers improved estimation tracking, especially when modeling uncertainties and disturbances are present.

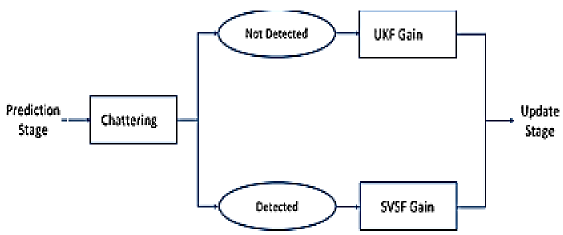

Figure 12 – The UK-SVSF estimation process [65].

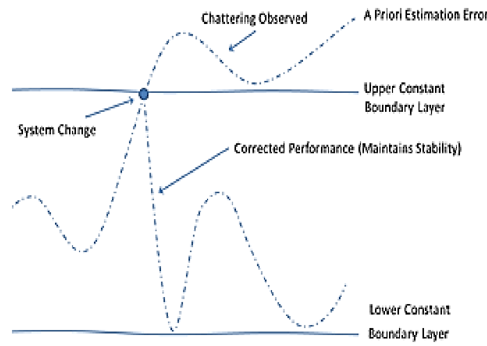

Figure 13 – Illustration of the combined UK-SVSF methodology [65].

4.4. The Proposed Unscented Smooth Variable Structure Filter

A significant amount of work has been performed since 2011 in an effort to improve the performance of the SVSF by varying the SBL width [49, 63 and 67]. In this work, we propose combining a SVSF with a UKF by utilizing a time-varying smooth boundary layer (SBL). In [49], two filters were implemented as shown in Figure 14. The first filter was implemented with a zero width SBL to maintain stability. The second filter was used to refine the estimate by using a time-varying SBL derived to satisfy equation (27).

$$\mathrm{J} = \left(\mathbf{e}_{x,2_{k|k}}\mathbf{e}_{x,2_{k|k}}^{T}\right) = \left(\mathbf{e}_{z,2_{k|k}} - \mathbf{v}_{k}\right)\left(\mathbf{e}_{z,2_{k|k}} - \mathbf{v}_{k}\right)^{T} \tag{27}$$

Where $\mathbf{e}_{z,2_{k|k}}$ is the a priori measurement estimation error for the second filter and is defined as:

$$\mathbf{e}_{z,2_{k|k}} = \mathbf{e}_{z,2_{k|k-1}} - \mathbf{K}_{SVSF} = \mathbf{e}_{z,2_{k|k-1}} - \left(\left|\mathbf{e}_{z,2_{k|k-1}}\right| + \boldsymbol{\gamma}\left|\mathbf{e}_{z,2_{k-1|k-1}}\right|\right)\circ \boldsymbol{sat}\left(\frac{\mathbf{e}_{z,1_{k|k-1}}}{\boldsymbol{\Psi}_{\mathrm{tv}_k}}\right) \tag{28}$$

Without losing generality, and for simplicity, assume $\mathbf{e}_{z,2_{k|k-1}} = \mathbf{e}_{z,1_{k|k-1}}$ (they have the same a posteriori estimates, $\mathbf{S}_{at} = \mathrm{diag}\left(\frac{\left|\mathbf{e}_{z,1_{k|k-1}}\right|}{\boldsymbol{\Psi}_{\mathrm{tv}_k}}\right)$ and $\boldsymbol{\gamma} = \mathbf{0}$ yields

$$\mathbf{S}_{at} = diag\left(\frac{\mathbf{e}_{z,1_{k|k-1}}}{\boldsymbol{\Psi}_{\mathrm{tv}_k}}\right) = \left(\mathbf{P}_{zz_{1,k|k-1}} - \mathbf{R}_k\right)\circ\mathbf{I}_{nxn}\left(\left(\mathbf{P}_{zz_{1,k|k-1}}\circ\mathbf{I}_{nxn}\right)\right)^{-1} \tag{29}$$

$$\boldsymbol{\Psi}_{\mathrm{tv}_k} = \left(\mathbf{P}_{zz_{1,k|k-1}}\circ\mathbf{I}_{nxn}\right)\left(\left(\mathbf{P}_{zz_{1,k|k-1}} - \mathbf{R}_k\right)\circ\mathbf{I}_{nxn}\right)^{-1}\left|\mathbf{e}_{z,1_{k|k-1}}\right| \tag{30}$$

where $\mathbf{e}_{\mathbf{z},\mathbf{1}_{k|k-1}}$ and $\mathbf{P}_{\mathbf{zz}_{1,k|k-1}}$ are the a priori measurement estimation error and state error covariance matrix, respectively (for the first filter). In [49], a linear system was considered; whereas in this paper, the system is nonlinear. In order to implement the UK-SVSF on a nonlinear system, a modification to the method is required:

calculation of the required covariance matrix using the UKF. In this case, it is proposed that the a posteriori covariance matrix is reduced to the measurement covariance matrix ($\mathbf{R}$) only. The a priori state error covariance matrix can be obtained from Figure 8. The required SBL may be calculated using equation (30). Note that the proposed strategy makes use of an inversion applied to a diagonal matrix, which reduces computational time and removes any ill-matrix conditions.

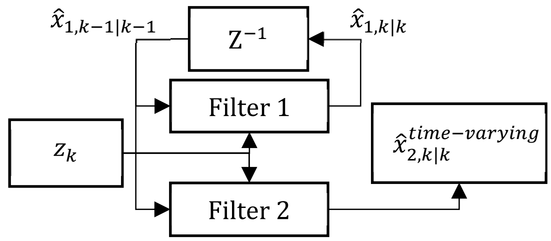

Figure 14 – The proposed (new) UK-SVSF structure [49].

5. Results of Combined Nonlinear Control/Estimation Applied to the PRRR Robot

In this paper, a PRRR robotic system was used to study and compare estimation strategies combined with nonlinear control. The end effector of a robotic arm was designed to move from an initial position and orientation to a final position and orientation. The inverse kinematics solutions for the required start and end positions were calculated using equations (2 – 10). The desired prismatic and revolute joint trajectories are shown in Figure 5.

This section discusses the results of applying the UKF, SVSF, UK-SVSF [65,66] and the proposed UK-SVSF to the nonlinear PRRR robot system. The estimation strategies were combined to the SMC and the overall performance was studied. The combined strategies were applied with and without the presence of modeling uncertainties at different noise level. Moreover, two scenarios were used, one with full rank measurement matrix and the other where only position and angles are measured. This leads to a total of 36 cases to be considered: 18 cases with modeling uncertainties (up to 50%), and 18 cases with no uncertainties. Each 18-case group has 9 cases with full ranked measurement matrix and 9 cases with only position and angles were measured. Each case represents a different combination of system and measurement noise's maximum amplitudes. Those amplitudes are:

$$\begin{gathered}(\mathrm{W_{max}}, \mathrm{V_{max}}) = (10^{-6}, 10^{-12}), (10^{-6}, 10^{-8}), (10^{-4}, 10^{-8}), (10^{-4}, 10^{-6}), \\ (10^{-2}, 10^{-6}), (10^{-2}, 10^{-3}), (10^{0}, 10^{-3}), (10^{1}, 10^{-3}) \text{ and } (10^{2}, 10^{-3})\end{gathered} \tag{31}$$

The error between the desired and measured states and their corresponding derivatives for few cases; i.e. cases 9, 18, 27, and 36 are illustrated in Figure 16 through Figure 31, and the root mean square error is computed for all cases is shown in Table 4. The results of the four implemented filter/control systems were similar when a small amount of noise was used and without the presence of modeling uncertainties. However, the UKF was unstable when only a few measurements were made available. i.e., the UKF became unstable under measurement uncertainties. The same result occurred when the noise amplitude was high. While comparing the standard SVSF, the previously published UK-SVSF, and the proposed UK-SVSF, the following observations were made:

1- Increasing the noise amplitude (particularly the system noise) reduces the filters performance in terms of estimation accuracy. The SVSF and the previously published UK-SVSF become unstable when the noise amplitude was increased. However, the proposed UK-SVSF implementation showed a significantly improved resistance towards noise.

2- Increasing the modeling uncertainty in the system improves the performance of the filters. This is due to the presence of chattering. When chattering is present, most of the signals are recovered and less filtering is required. In this case, the information provided to the controller will have more knowledge and information about the true status of the system. However, the performance decays with increasing the noise amplitude (as expected).

3- Decreasing the number of measured states reduces the overall performance. In this case, the UKF did not yield a stable or reliable result.

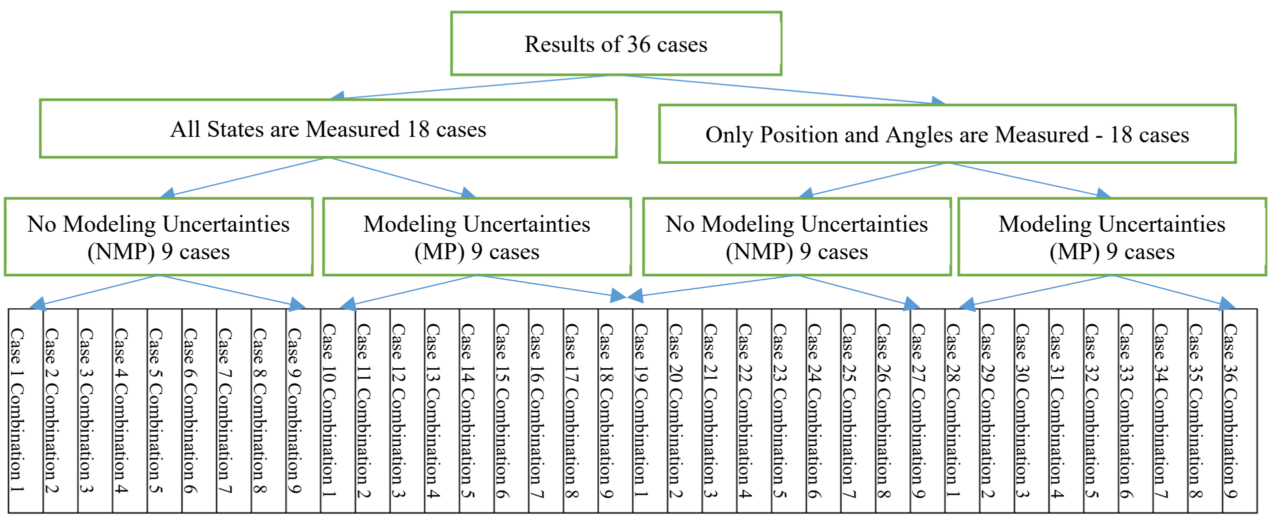

Figure 15 – Distribution of the 36 cases considered

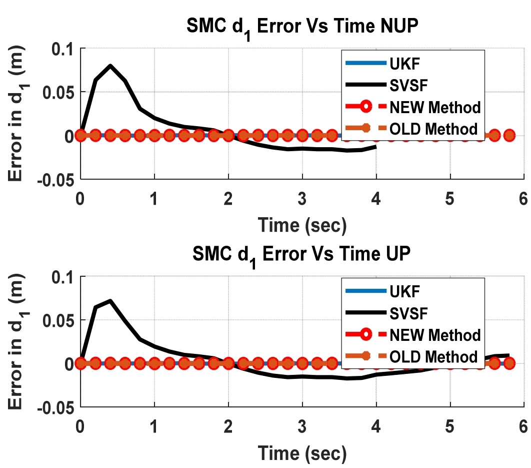

Figure 16 – The error in first state between the desired and the measured for cases 9 & 18

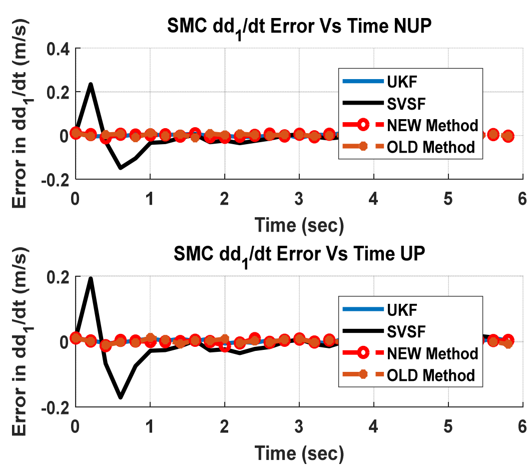

Figure 17 – The error in second state between the desired and the measured for cases 9 & 18

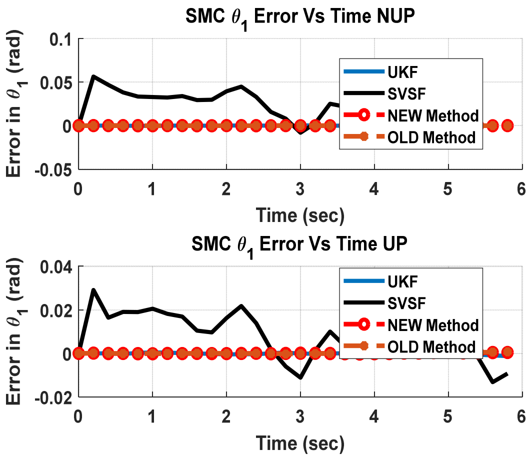

Figure 18 – The error in third state between the desired and the measured for cases 9 & 18

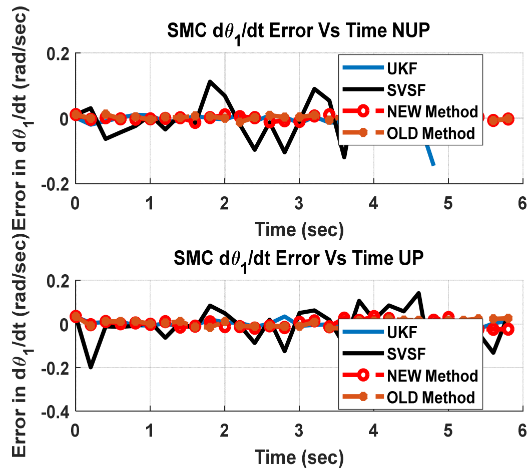

Figure 19 – The error in fourth state between the desired and the measured for cases 9 & 18

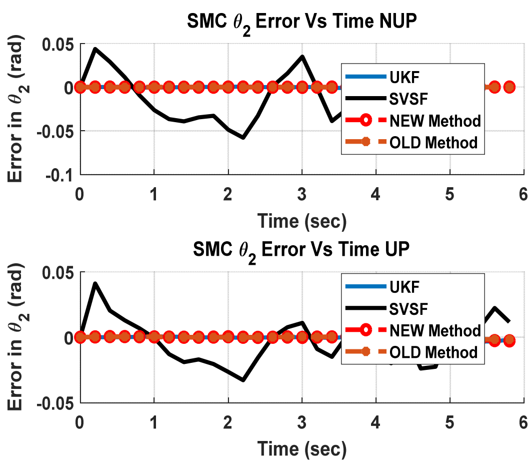

Figure 20 – The error in fifth state between the desired and the measured for cases 9 & 18

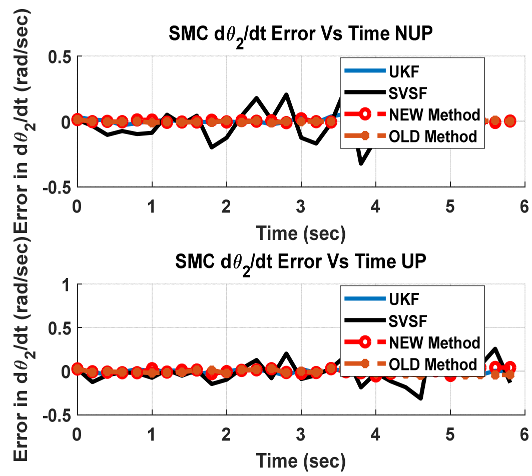

Figure 21 – The error in sixth state between the desired and the measured for cases 9 & 18

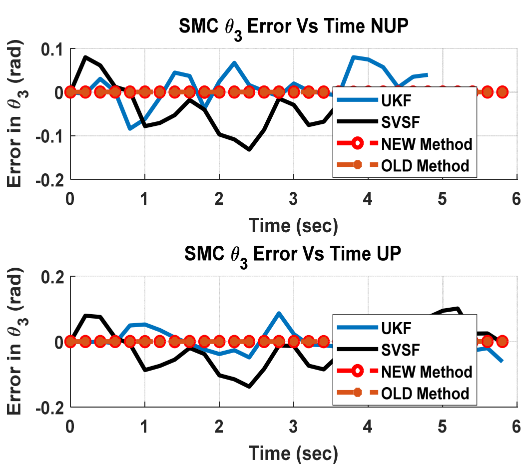

Figure 22 – The error in seventh state between the desired and the measured for cases 9 & 18

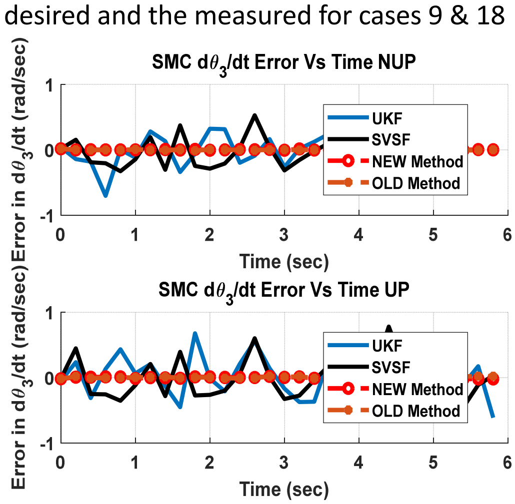

Figure 23 – The error in eigthth state between the desired and the measured for cases 9 & 18

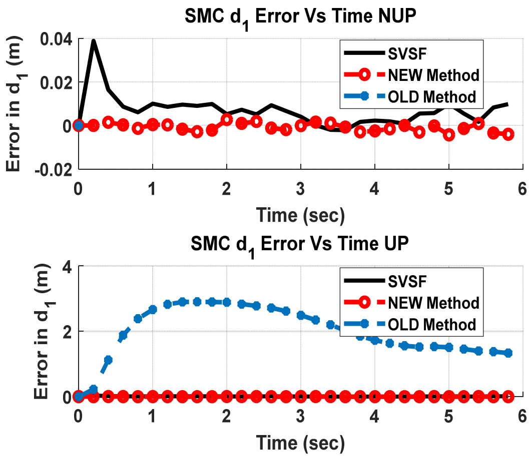

Figure 24 – The error in first state between the desired and the measured for cases 27 & 36

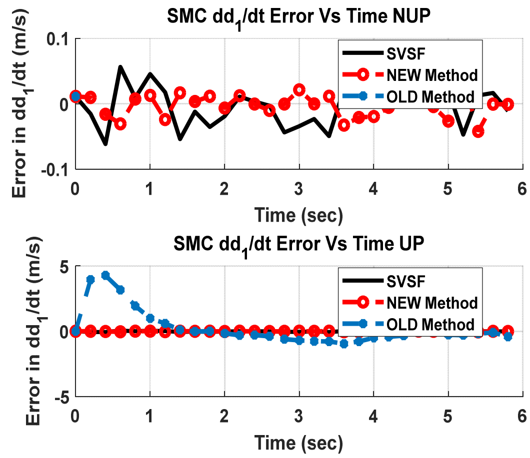

Figure 25 – The error in second state between the desired and the measured for cases 27 & 36

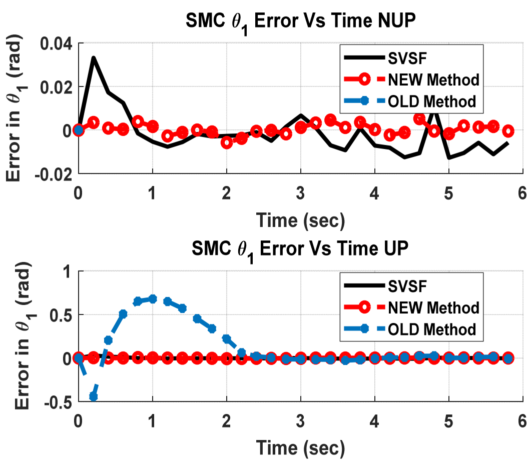

Figure 26 – The error in third state between the desired and the measured for cases 27 & 36

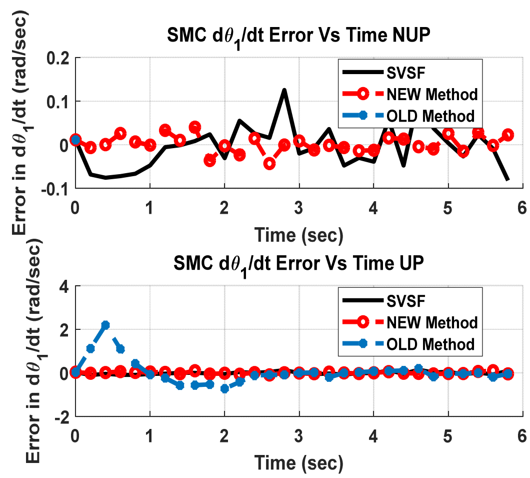

Figure 27 – The error in fourth state between the desired and the measured for cases 27 & 36

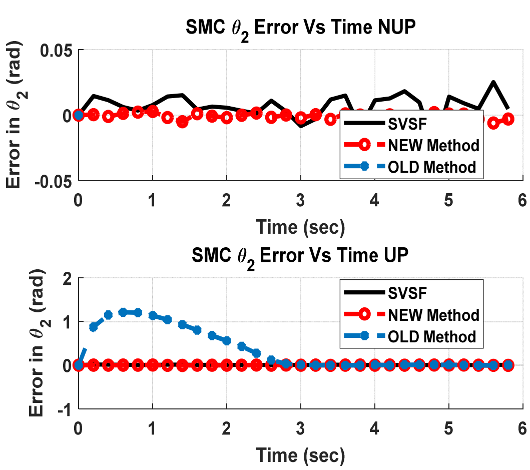

Figure 28 – The error in fifth state between the desired and the measured for cases 27 & 36

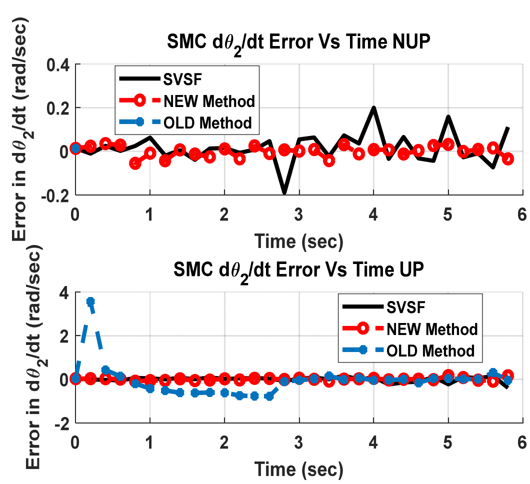

Figure 29 – The error in sixth state between the desired and the measured for cases 27 & 36

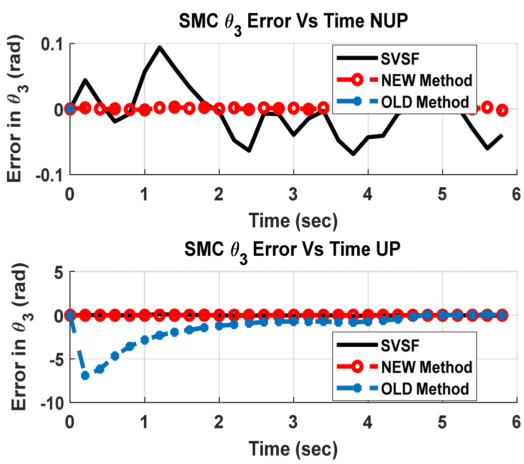

Figure 30 – The error in seventh state between the desired and the measured for cases 27 & 36

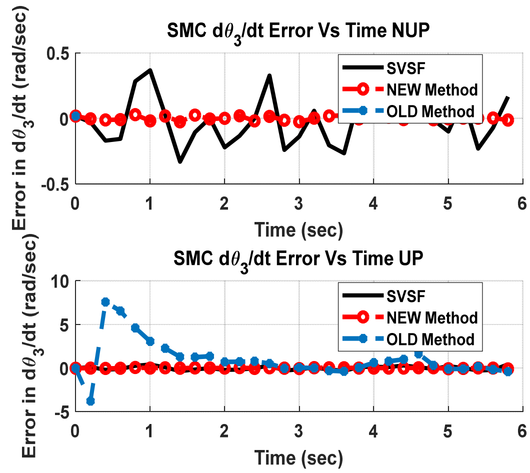

Figure 31 – The error in eigthth state between the desired and the measured for cases 27 & 36

Table 4 – RMSE results for PRRR estimation.

			No Modeling Uncertainties (NUP) $\times 10^{-6}$								Modeling Uncertainties (UP) $\times 10^{-6}$							
			State 1	State 2	State 3	State 4	State 5	State 6	State 7	State 8	State 1	State 2	State 3	State 4	State 5	State 6	State 7	State 8
First Combination	ALL Measured	UKF	2.4	37	2.8	53	2.5	56	1.2	28	NaN	NaN	NaN	NaN	NaN	NaN	NaN	NaN
		SVSF	2.4	37	2.8	53	2.5	56	1.2	28	0.9	32	7.2	200	17	340	6.5	180
		OLD	2.4	37	2.8	53	2.5	56	1.2	28	0.9	32	7.2	200	17	340	6.5	180
		NEW	2.4	37	2.8	53	2.5	56	1.2	28	0.9	32	7.2	200	17	340	6.5	180
	Position & Angles are Measured	UKF	NaN	NaN	NaN	NaN	NaN	NaN	NaN	NaN	NaN	NaN	NaN	NaN	NaN	NaN	NaN	NaN
		SVSF	1	57	2.1	110	1.8	120	1	59	0.8	62	8.7	410	17	670	6.6	350
		OLD	2.6	62	3.1	110	1.7	110	1.8	60	0.9	61	8.8	420	18	680	6.1	340
		NEW	1.1	70	1.5	110	2.1	110	1	60	0.8	62	8.7	410	17	670	6.5	350
Second Combination	ALL Measured	UKF	3.1	76	7.7	160	2.9	76	1.8	38	NaN	NaN	NaN	NaN	NaN	NaN	NaN	NaN
		SVSF	2.4	37	2.8	53	2.5	56	1.2	28	0.9	32	7.2	200	17	340	6.5	180
		OLD	2.4	37	2.8	53	2.5	56	1.2	28	1.1	31	8.2	200	15	340	7.6	180
		NEW	2.4	37	2.8	53	2.5	57	1.3	29	0.9	31	8.1	200	15	340	7.5	180
	Position & Angles are Measured	UKF	NaN	NaN	NaN	NaN	NaN	NaN	NaN	NaN	NaN	NaN	NaN	NaN	NaN	NaN	NaN	NaN
		SVSF	1.1	70	1.5	110	2.1	110	1	60	0.9	61	8.7	410	18	680	6.1	330
		OLD	1.9	50	4.4	84	1.4	84	1.7	46	0.9	61	8.7	410	18	680	6.1	330
		NEW	0.8	52	1.3	100	0.8	120	1	68	1.1	61	9.1	420	17	680	6.2	330
Third Combination	ALL Measured	UKF	2.4	37	2.8	53	2.5	56	1.2	28	NaN	NaN	NaN	NaN	NaN	NaN	NaN	NaN
		SVSF	2.4	37	2.8	53	2.5	57	1.2	28	0.9	32	7.2	200	17	340	6.5	180
		OLD	2.4	37	2.8	53	2.5	56	1.2	28	0.9	32	7.2	200	17	340	6.5	180
		NEW	2.4	37	2.8	53	2.5	56	1.2	28	0.9	32	7.2	200	17	340	6.5	180
	Position & Angles are Measured	UKF	NaN	NaN	NaN	NaN	NaN	NaN	NaN	NaN	NaN	NaN	NaN	NaN	NaN	NaN	NaN	NaN
		SVSF	1	69	2.1	110	1.8	110	1	58	0.8	62	8.7	410	17	670	6.6	350
		OLD	0.9	37	1.6	120	1.2	85	0.6	37	0.8	62	8.8	410	17	670	6.6	350
		NEW	1.9	59	1.8	110	1.5	110	1.9	61	1	60	9.4	410	17	680	7	330

			No Modeling Uncertainties (NUP) $\times 10^{-6}$								Modeling Uncertainties (UP) $\times 10^{-6}$							
			State 1	State 2	State 3	State 4	State 5	State 6	State 7	State 8	State 1	State 2	State 3	State 4	State 5	State 6	State 7	State 8
Fourth Combination	ALL Measured	UKF	3.1	76	7.7	160	2.9	76	1.8	38	NaN	NaN	NaN	NaN	NaN	NaN	NaN	NaN
		SVSF	2.4	37	2.8	53	2.5	57	1.2	28	0.9	32	7.2	200	17	340	6.5	180
		OLD	2.4	37	2.8	53	2.5	56	1.2	28	1.3	33	9.2	210	15	340	6.6	180
		NEW	2.4	37	2.8	53	2.5	57	1.3	29	0.9	31	8.1	200	15	340	7.5	180
	Position & Angles are Measured	UKF	NaN	NaN	NaN	NaN	NaN	NaN	NaN	NaN	NaN	NaN	NaN	NaN	NaN	NaN	NaN	NaN
		SVSF	0.8	64	1.3	110	1.5	110	0.6	63	0.8	61	8.4	410	18	680	5.6	330
		OLD	0.7	62	2.3	110	1.4	110	0.6	55	0.9	61	7	420	20	680	5.6	340
		NEW	0.7	67	1.2	110	0.9	110	0.8	54	0.6	62	8.5	410	16	680	5.9	340
Fifth Combination	ALL Measured	UKF	2.3	38	3.1	55	2.6	54	1.3	30	NaN	NaN	NaN	NaN	NaN	NaN	NaN	NaN
		SVSF	2.4	38	3.1	56	2.7	55	1.6	30	1.1	31	10	200	21	340	9.1	180
		OLD	2	39	3.2	55	2.6	55	1.4	30	1	31	9.9	200	21	340	9.1	180
		NEW	1.9	39	3.2	55	2.6	55	1.5	30	0.9	32	7.2	200	16	340	6.5	180
	Position & Angles are Measured	UKF	NaN	NaN	NaN	NaN	NaN	NaN	NaN	NaN	NaN	NaN	NaN	NaN	NaN	NaN	NaN	NaN
		SVSF	1	57	1.7	110	1.6	120	0.7	60	0.9	60	8.2	410	20	680	7.4	330
		OLD	1.6	35	0.8	59	1.5	60	1.3	33	1	60	9	410	17	670	10	330
		NEW	0.7	66	1.4	110	1.1	110	0.5	65	0.7	61	9.6	410	17	680	6.1	340
Sixth Combination	ALL Measured	UKF	65	480	220	High	120	High	28	280	NaN	NaN	NaN	NaN	NaN	NaN	NaN	NaN
		SVSF	1.3	36	1.8	61	1.9	59	1	32	0.8	35	3.6	200	2.8	300	4.9	150
		OLD	1	40	2.1	63	1.8	61	0.7	36	1.1	37	2.4	210	17	320	1.2	170
		NEW	1	59	0.9	89	0.8	87	0.9	61	0.9	58	2.1	220	14	350	2.5	180
	Position & Angles are Measured	UKF	NaN	NaN	NaN	NaN	NaN	NaN	NaN	NaN	NaN	NaN	NaN	NaN	NaN	NaN	NaN	NaN
		SVSF	36	240	33	360	37	350	26	220	40	240	35	760	49	990	27	530
		OLD	30	220	34	340	36	380	31	240	34	230	33	750	41	1000	40	590
		NEW	28	210	28	340	37	330	28	210	30	210	33	720	38	930	29	510
Seventh Combination	ALL Measured	UKF	1	55	0.7	84	0.8	85	0.9	58	NaN	NaN	NaN	NaN	NaN	NaN	NaN	NaN
		SVSF	1.2	35	3.5	64	5.6	76	6.4	60	1.1	37	8.6	190	6.1	270	11	150
		OLD	1	56	0.7	84	0.8	85	0.7	57	1	56	5.1	210	12	350	4.1	180
		NEW	1.2	60	0.8	88	0.8	89	0.8	58	1.2	59	1.9	220	12	350	3.4	180
	Position & Angles are Measured	UKF	NaN	NaN	NaN	NaN	NaN	NaN	NaN	NaN	NaN	NaN	NaN	NaN	NaN	NaN	NaN	NaN
		SVSF	53	330	51	510	47	450	41	290	53	330	54	900	56	High	54	640
		OLD	31	270	47	460	39	520	51	380	31	300	54	890	64	High	49	680
		NEW	32	210	33	340	40	340	18	200	34	210	34	710	39	940	34	510

			No Modeling Uncertainties (NUP) $\times 10^{-6}$								Modeling Uncertainties (UP) $\times 10^{-6}$							
			State 1	State 2	State 3	State 4	State 5	State 6	State 7	State 8	State 1	State 2	State 3	State 4	State 5	State 6	State 7	State 8
Eighth Combination	ALL Measured	UKF	1.1	63	0.7	91	0.9	100	2	110	NaN	NaN	NaN	NaN	NaN	NaN	NaN	NaN
		SVSF	31	170	43	260	46	330	65	430	31	170	44	300	32	320	64	500
		OLD	0.9	59	0.9	88	0.8	89	0.8	60	1	60	2	220	16	360	2.2	180
		NEW	1.1	59	0.9	88	0.9	87	0.8	59	0.9	60	3.1	220	12	350	4.3	180
	Position & Angles are Measured	UKF	NaN	NaN	NaN	NaN	NaN	NaN	NaN	NaN	NaN	NaN	NaN	NaN	NaN	NaN	NaN	NaN
		SVSF	41	450	55	590	44	600	44	440	43	460	55	High	45	High	53	980
		OLD	NaN	NaN	NaN	NaN	NaN	NaN	NaN	NaN	58	250	45	680	100	High	150	High
		NEW	22	210	36	330	26	320	35	240	21	210	40	690	30	910	35	510
Ninth Combination	ALL Measured	UKF	NaN	NaN	NaN	NaN	NaN	NaN	NaN	NaN	NaN	NaN	NaN	NaN	NaN	NaN	NaN	NaN
		SVSF	NaN	NaN	NaN	NaN	NaN	NaN	NaN	NaN	290	940	210	High	230	High	890	High
		OLD	1.1	59	0.8	88	0.9	87	0.8	60	1	60	3.3	220	11	350	3	180
		NEW	1	60	0.8	88	0.9	88	0.9	60	1	58	2.4	220	13	360	2.2	180
	Position & Angles are Measured	UKF	NaN	NaN	NaN	NaN	NaN	NaN	NaN	NaN	NaN	NaN	NaN	NaN	NaN	NaN	NaN	NaN
		SVSF	130	700	130	High	150	High	510	High	120	680	110	High	86	High	520	High
		OLD	NaN	NaN	NaN	NaN	NaN	NaN	NaN	NaN	High	High	High	High	High	High	High	High
		NEW	27	240	33	360	29	330	33	230	29	240	39	720	29	900	35	510

6. Conclusions and Future Work

In this paper, a four-DOF robotic system was used as the testbed to evaluate a control system comprised of a nonlinear sliding mode controller (SMC) and four different estimation strategies. The four estimation strategies considered were: the unscented Kalman filter (UKF), smooth variable structure filter (SVSF), a previously published unscented smooth variable structure filter (UK-SVSF), and the proposed new version of the UK-SVSF. Modeling uncertainties were introduced in an effort to study and compare the performance of the control system. In the presence of modeling uncertainties and/or fewer measured states, the UKF failed to yield an estimate for the state trajectories. The other three filters showed relatively high resistance to modeling uncertainties. However, these methods were extremely sensitive to system and measurement noise. The SVSF and the previously published UK-SVSF yielded good tracking results; however, the proposed UK-SVSF estimation strategy yielded the best estimation results in terms of RMSE when the noise amplitude became relatively high. Future work will look at implementing the SMC and UK-SVSF on an industrial PRRR robot currently being installed for experimentation.

APPENDIX 1

Commonly used nomenclature in this paper is summarized as follows:

$.^{-1}\ .^{+}\ .^{T}$: Inverse, pseudo inverse and transpose, respectively.

|ABS|, ^: Absolute and estimated values, respectively.

$(\mathbf{a})_i$: The i row of $\mathbf{a}$.

$A \circ B$: Schur product between A and B.

a_{i-1} : Link-i length (m).

α_{i-1} : Link-i twist (rad).

c_i : $\cos(\theta_i)$.

c_{ij} : $\cos(\theta_i + \theta_j)$.

d_i : Link-i offset (m).

$\mathbf{e_m}$: The estimation error vectors.

$\mathbf{f}(.)$: The system's model function.

F_z : Prismatic joint-1 motor force (N).

$\boldsymbol{\gamma}$: The SVSF's positive constant matrix.

g : Gravity acceleration (m/s2).

$\mathbf{g}(.)$: The sensor's model function.

i, j: Subscripts used to identify elements.

$\mathbf{I}_{n\times n}$: The identity matrix with dimensions of $\mathrm{n} \times \mathrm{n}$.

k: Time step value.

$k|k-1$: The a priori value at time k.

$k|k$: The a posteriori value at time k.

$\mathbf{K}_{SVSF}$: The correction gain of the SVSF.

$\mathbf{M}(\Theta)$: Inertia matrix.

$m_1, m_2 \ldots m_5$: masses of links 1, 2, 3 and 4 respectively (kg).

m, n: Number of measurements and states, respectively.

$\mathbf{P}_{\mathrm{zz}}$: The output's error covariance matrix.

$\mathbf{P}$: The error covariance matrix.

P_x, P_y, P_z: Cartesian coordinates of the E.E in world frame (m).

q : The number of the sigma points, $2n+1$.

$\boldsymbol{\Psi}$: The smoothing boundary layer vector.

$\boldsymbol{\Psi}_{tv}$: The time-varying smoothing boundary layer vector.

$\mathbf{Q}$: The process noise covariance matrix.

$\mathbf{R}$: The measurements noise covariance matrix.

$\mathbb{R}^{a \times b}$: Space dimension of size a $\times$ b.

$RMSE$: The root mean square error.

s_i: $\sin(\theta_i)$.

s_{ij}: $\sin(\theta_i + \theta_j)$.

$\mathbf{sat}(\mathbf{a}, \mathbf{b})$: The saturated function of $\mathbf{a}$ using the BL $\mathbf{b}$.

$sat(a, b)$: The saturated function of element a using the BL b.

$\mathbf{S}_{\boldsymbol{at}}(\mathbf{a}, \mathbf{b})$: The absolute diagonal matrix of $\mathbf{sat}(\mathbf{a}, \mathbf{b})$.

$\mathbf{sgn}(\mathbf{a})$: The sign function of the vector $\mathbf{a}$.

$sgn(a)$: The sign function of the element a.

T_s: Sampling time.

θ_i: Joint-i angle (rad).

$\boldsymbol{\tau}$: Joints force and torques vector.

τ_i : Revolute joint-i motor torque (N.M).

u: The input.

$V(\Theta, \dot{\Theta})$: Viscous friction vector.

$\mathbf{v}, \mathbf{w}$: The measurement and system noise, respectively.

W_i: The assigned weight, $W_i = \begin{cases} 0 & i = 0 \\ \frac{1}{2n} & i \neq 0 \end{cases}$.

$\mathbf{x}$: The state vector.

$\mathbf{z}_k$: The output vector.

$\mathbf{X}_i, \mathbf{Z}_i$: The estimate and its measurement for the i^{th} sigma point, respectively.

Ξ_k: The alternative measurement vector.

APPENDIX 2

Additional equations that describe the robot dynamics are as follows:

$$\tau_i = \frac{d}{dt}\left(\frac{\partial L}{\partial \dot{\Theta}_i}\right) - \left(\frac{\partial L}{\partial \Theta_{\mathrm{i}}}\right) \tag{2.1}$$

$$L = \sum(Kinetic - Potential) = \sum\left(\frac{1}{2} m_i \, {}^{0}_{c_i}v^T \, {}^{0}_{c_i}v + \frac{1}{2} \, {}^{0}_{c_i}\omega^T I_i \, {}^{0}_{c_i}\omega + m_i \mathbf{g}^{0^T} \, {}^{0}_{c_i}r\right) \text{ where } \mathbf{g}^0 = \begin{bmatrix} 0 \\ 0 \\ -g \end{bmatrix} \tag{2.2}$$

$$\boldsymbol{\tau} = \mathbf{M}(\boldsymbol{\Theta})\ddot{\boldsymbol{\Theta}} + \mathbf{V}(\boldsymbol{\Theta}, \dot{\boldsymbol{\Theta}}) + \mathbf{G}(\boldsymbol{\Theta}) \tag{2.3}$$

Assume that the links are homogeneous, where the center of any link's mass located at the middle of that link. The location of each mass, ${}^{0}_{c_i}r, i = 1, 2, 3, 4$ and 5, with respect to frame **0** is then defined as follows:

$${}^{0}_{c_1}r = \begin{bmatrix} \frac{a_1}{2} \\ 0 \\ d_1 \end{bmatrix} \tag{2.4}$$

$${}^{0}_{c_2}r = \begin{bmatrix} a_1 + \frac{a_2}{2} c_1 \\ a_1 + \frac{a_2}{2} s_1 \\ d_1 \end{bmatrix} \tag{2.5}$$

$${}^{0}_{c_3}r = \begin{bmatrix} a_1 + a_2 c_1 + \frac{a_3}{2} c_{12} \\ a_1 + a_2 s_1 + \frac{a_3}{2} s_{12} \\ d_1 \end{bmatrix} \tag{2.6}$$

$${}^{0}_{c_4}r = \begin{bmatrix} a_1 + a_2 c_1 + a_3 c_{12} \\ a_1 + a_2 s_1 + a_3 s_{12} \\ d_1 \end{bmatrix} \tag{2.7}$$

$$\text{and } {}^{0}_{c_5}r = \begin{bmatrix} a_1 + a_2 c_1 + a_3 c_{12} \\ a_1 + a_2 s_1 + a_3 s_{12} \\ d_1 - d_2 \end{bmatrix} \tag{2.8}$$

The velocity of each mass can be obtained by taking the derivative of equations (2.4 to 2.8) as follows:

$${}^{0}_{c_1}v = \begin{bmatrix} 0 \\ 0 \\ \dot{d}_1 \end{bmatrix} \tag{2.9}$$

$$ {}_{c_2}^{0}v = \begin{bmatrix} -\frac{a_2}{2} s_1 \dot{\theta}_1 \\ \frac{a_2}{2} c_1 \dot{\theta}_1 \\ \dot{d}_1 \end{bmatrix} \tag{2.10} $$

$$ {}_{c_3}^{0}v = \begin{bmatrix} -a_2 s_1 \dot{\theta}_1 - \frac{a_3}{2} s_{12}(\dot{\theta}_1 + \dot{\theta}_2) \\ a_2 c_1 \dot{\theta}_1 + \frac{a_3}{2} c_{12}(\dot{\theta}_1 + \dot{\theta}_2) \\ \dot{d}_1 \end{bmatrix} \tag{2.11} $$

$$ {}_{c_4}^{0}v = \begin{bmatrix} -a_2 s_1 \dot{\theta}_1 - a_3 s_{12}(\dot{\theta}_1 + \dot{\theta}_2) \\ a_2 c_1 \dot{\theta}_1 + a_3 c_{12}(\dot{\theta}_1 + \dot{\theta}_2) \\ \dot{d}_1 \end{bmatrix} \tag{2.12} $$

$$ \text{and } {}_{c_5}^{0}v = \begin{bmatrix} -a_2 s_1 \dot{\theta}_1 - a_3 s_{12}(\dot{\theta}_1 + \dot{\theta}_2) \\ a_2 c_1 \dot{\theta}_1 + a_3 c_{12}(\dot{\theta}_1 + \dot{\theta}_2) \\ \dot{d}_1 \end{bmatrix} \tag{2.13} $$

The angular velocity of each link can be obtained as follows:

$$ {}_{c_1}^{0}\omega = \begin{bmatrix} 0 \\ 0 \\ 0 \end{bmatrix} \tag{2.14} $$

$$ {}_{c_2}^{0}\omega = \begin{bmatrix} 0 \\ 0 \\ \dot{\theta}_1 \end{bmatrix} \tag{2.15} $$

$$ {}_{c_3}^{0}\omega = \begin{bmatrix} 0 \\ 0 \\ \dot{\theta}_1 + \dot{\theta}_2 \end{bmatrix} \tag{2.16} $$

$$ {}_{c_4}^{0}\omega = \begin{bmatrix} 0 \\ 0 \\ \dot{\theta}_1 + \dot{\theta}_2 + \dot{\theta}_3 \end{bmatrix} \tag{2.17} $$

$$ \text{and } {}_{c_5}^{0}\omega = \begin{bmatrix} 0 \\ 0 \\ \dot{\theta}_1 + \dot{\theta}_2 + \dot{\theta}_3 \end{bmatrix} \tag{2.18} $$

The energies of equation (2.2) can be obtained as follows:

$$ \frac{1}{2} m_1 {}_{c_1}^{0}v^T {}_{c_1}^{0}v = \frac{1}{2} m_1 \dot{d}_1^2 \tag{2.19} $$

$$ \frac{1}{2} m_2 {}_{c_2}^{0}v^T {}_{c_2}^{0}v = \frac{1}{2} m_2 \left(\frac{a_2^2}{4} \dot{\theta}_1^2 + \dot{d}_1^2 \right) \tag{2.20} $$

$$\frac{1}{2}m_3\, {}^{0}_{c_3}v^T\, {}^{0}_{c_3}v = \frac{1}{2}m_3\left(a_2^2\dot{\theta}_1^2 + \frac{a_3^2}{4}\left(\dot{\theta}_1 + \dot{\theta}_2\right)^2 + a_2a_3c_2\dot{\theta}_1\left(\dot{\theta}_1 + \dot{\theta}_2\right) + \dot{d}_1^2\right) \tag{2.21}$$

$$\frac{1}{2}(m_4 + m_5)\, {}^{0}_{c_4}v^T\, {}^{0}_{c_4}v = \frac{1}{2}(m_4 + m_5)\left(\left(a_2\dot{\theta}_1\right)^2 + \left(a_3\left(\dot{\theta}_1 + \dot{\theta}_2\right)\right)^2 + 2a_2c_2\dot{\theta}_1a_3\left(\dot{\theta}_1 + \dot{\theta}_2\right) + \dot{d}_1^2\right) \tag{2.22}$$

$$\frac{1}{2}\, {}^{0}_{c_1}\omega^T I_1\, {}^{0}_{c_1}\omega = 0 \tag{2.23}$$

$$\frac{1}{2}\, {}^{0}_{c_2}\omega^T I_2\, {}^{0}_{c_2}\omega = \frac{1}{2}I_{zz2}\dot{\theta}_1^2 \tag{2.24}$$

$$\frac{1}{2}\, {}^{0}_{c_3}\omega^T I_3\, {}^{0}_{c_3}\omega = \frac{1}{2}I_{zz3}\left(\dot{\theta}_1 + \dot{\theta}_2\right)^2 \tag{2.25}$$

$$\frac{1}{2}\, {}^{0}_{c_4}\omega^T (I_4 + I_5)\, {}^{0}_{c_4}\omega = \frac{1}{2}(I_{zz4} + I_{zz5})\left(\dot{\theta}_1 + \dot{\theta}_2 + \dot{\theta}_3\right)^2 \tag{2.26}$$

$$\text{and } m_i\mathbf{g}^{0^T}\, {}^{0}_{c_i}r = -m_i g d_1 \tag{2.27}$$

Substitute equations (2.19-2.27) in equation (2.2) yields the following:

$$L = -\sum_{i=1}^{4} m_i\, g d_1 + \begin{bmatrix} \frac{1}{2}m_1\dot{d}_1^2 + \frac{1}{2}m_2\left(\frac{a_2^2}{4}\dot{\theta}_1^2 + \dot{d}_1^2\right) \\ +\frac{1}{2}m_3\begin{pmatrix} a_2^2\dot{\theta}_1^2 + \frac{a_3^2}{4}\left(\dot{\theta}_1 + \dot{\theta}_2\right)^2 \\ +a_2a_3c_2\dot{\theta}_1\left(\dot{\theta}_1 + \dot{\theta}_2\right) + \dot{d}_1^2 \end{pmatrix} \\ +\frac{1}{2}(m_4 + m_5)\begin{pmatrix} \left(a_2\dot{\theta}_1\right)^2 + \left(a_3\left(\dot{\theta}_1 + \dot{\theta}_2\right)\right)^2 \\ +2a_2c_2\dot{\theta}_1a_3\left(\dot{\theta}_1 + \dot{\theta}_2\right) + \dot{d}_1^2 \end{pmatrix} \end{bmatrix} + \begin{bmatrix} \frac{1}{2}I_{zz2}\dot{\theta}_1^2 \\ +\frac{1}{2}I_{zz3}\left(\dot{\theta}_1 + \dot{\theta}_2\right)^2 \\ +\frac{1}{2}(I_{zz4} + I_{zz5})\left(\dot{\theta}_1 + \dot{\theta}_2 + \dot{\theta}_3\right)^2 \end{bmatrix} \tag{2.28}$$

Taking the derivative of equation (2.28) with respect to the variables leads to the following:

$$\frac{\partial L}{\partial \theta_1} = 0 \tag{2.29}$$

$$\frac{\partial L}{\partial \theta_2} = -\left(\frac{1}{2}m_3 + m_4 + m_5\right)a_2a_3s_2\dot{\theta}_1\left(\dot{\theta}_1 + \dot{\theta}_2\right) \tag{2.30}$$

$$\frac{\partial L}{\partial \theta_3} = 0 \tag{2.31}$$

$$\frac{\partial L}{\partial d_1} = -\sum_{i=1}^{5} m_i\, g = -m_T g \tag{2.32}$$

$$\frac{\partial L}{\partial \dot{\theta}_1} = \begin{bmatrix} \begin{pmatrix} m_2\frac{a_2^2}{4} + m_3a_2^2 + \frac{a_3^2}{4}m_3 + (m_4 + m_5){a_2}^2 + a_2a_3c_2m_3 + {a_3}^2(m_4 + m_5) \\ +2a_2a_3c_2(m_4 + m_5) + I_{zz2} + I_{zz3} + (I_{zz4} + I_{zz5}) \end{pmatrix}\dot{\theta}_1 \\ +\left(\frac{a_3^2}{4}m_3 + \frac{1}{2}a_2a_3c_2m_3 + {a_3}^2(m_4 + m_5) + a_2a_3c_2(m_4 + m_5) + I_{zz3} + (I_{zz4} + I_{zz5})\right)\left(\dot{\theta}_2\right) \\ +(I_{zz4} + I_{zz5})\left(\dot{\theta}_3\right) \end{bmatrix} \tag{2.33}$$

$$\frac{\partial L}{\partial \dot{\theta}_1} = A_1\dot{\theta}_1 + A_4\dot{\theta}_2 + A_5\dot{\theta}_3$$

$$A_1 = m_2\frac{a_2^2}{4} + m_3\left(a_2^2 + \frac{a_3^2}{4} + a_2a_3c_2\right) + (2a_2a_3c_2 + {a_2}^2 + {a_3}^2)(m_4 + m_5) + I_{zz2} + I_{zz3} + I_{zz4} + I_{zz5}$$

$$A_4 = \left(\frac{a_3^2}{4} + \frac{1}{2}a_2a_3c_2\right)m_3 + ({a_3}^2 + a_2a_3c_2)(m_4 + m_5) + I_{zz3} + I_{zz4} + I_{zz5}$$

$$A_5 = (I_{zz4} + I_{zz5})$$

$$\frac{d}{dt}\left(\frac{\partial L}{\partial \dot{\theta}_1}\right) = A_1\ddot{\theta}_1 + A_4\ddot{\theta}_2 + A_5\ddot{\theta}_3 + A_7$$

$$A_7 = -\big(m_3(a_2a_3s_2) + (2a_2a_3s_2)(m_4 + m_5)\big)\dot{\theta}_1\dot{\theta}_2 - (a_2a_3s_2)\left(\frac{1}{2}m_3 + m_4 + m_5\right)\dot{\theta}_2^2$$

$$\frac{\partial L}{\partial \dot{\theta}_2} = \begin{bmatrix} \left(\frac{1}{2}m_3\left(2\frac{a_3^2}{4} + a_2a_3c_2\right) + (m_4 + m_5)\big(a_3^2 + a_2c_2\dot{\theta}_1a_3\big) + (I_{zz4} + I_{zz5} + I_{zz3})\right)\dot{\theta}_1 \\ +\left(m_3\frac{a_3^2}{4} + (m_4 + m_5)a_3^2 + (I_{zz4} + I_{zz5} + I_{zz3})\right)\dot{\theta}_2 \\ +(I_{zz4} + I_{zz5})\big(\dot{\theta}_3\big) \end{bmatrix}$$

$$\frac{\partial L}{\partial \dot{\theta}_2} = A_4\dot{\theta}_1 + A_2\dot{\theta}_2 + A_6\dot{\theta}_3$$

$$A_4 = \left(m_3\left(\frac{a_3^2}{4} + \frac{1}{2}a_2a_3c_2\right) + (m_4 + m_5)\big(a_3^2 + a_2c_2\dot{\theta}_1a_3\big) + (I_{zz4} + I_{zz5} + I_{zz3})\right) \tag{2.34}$$

$$A_2 = \left(m_3\frac{a_3^2}{4} + (m_4 + m_5)a_3^2 + (I_{zz4} + I_{zz5} + I_{zz3})\right)$$

$$A_6 = (I_{zz4} + I_{zz5})$$

$$\frac{d}{dt}\left(\frac{\partial L}{\partial \dot{\theta}_2}\right) = A_4\ddot{\theta}_1 + A_2\ddot{\theta}_2 + A_6\ddot{\theta}_3 + A_8$$

$$A_8 = -\left(\frac{1}{2}m_3(a_2a_3s_2) + (a_2a_3s_2)(m_4 + m_5)\right)\dot{\theta}_1\dot{\theta}_2$$

$$\frac{\partial L}{\partial \dot{\theta}_3} = (I_{zz4} + I_{zz5})\big(\dot{\theta}_1 + \dot{\theta}_2 + \dot{\theta}_3\big)$$

$$\frac{\partial L}{\partial \dot{\theta}_3} = A_5\dot{\theta}_1 + A_6\dot{\theta}_2 + A_3\dot{\theta}_3 \tag{2.35}$$

$$A_3 = A_5 = A_6 = (I_{zz4} + I_{zz5})$$

$$\frac{d}{dt}\left(\frac{\partial L}{\partial \dot{\theta}_3}\right) = A_5\ddot{\theta}_1 + A_6\ddot{\theta}_2 + A_3\ddot{\theta}_3$$

$$\frac{\partial L}{\partial \dot{d}_1} = m_1\dot{d}_1 + m_2\dot{d}_1 + m_3\dot{d}_1 + m_4\dot{d}_1 + m_5\dot{d}_1 = m_T\dot{d}_1 \rightarrow \frac{d}{dt}\left(\frac{\partial L}{\partial \dot{d}_1}\right) = m_T\ddot{d}_1 \tag{2.36}$$

Substitute equations (2.29 to 2.36) in equation (2.1) and rearrange to have the shape of equation (2.3) give the following parameters:

$$\boldsymbol{\tau} = \begin{bmatrix} F \\ \tau_1 \\ \tau_2 \\ \tau_3 \end{bmatrix} \tag{2.37}$$

$$\mathbf{M}(\boldsymbol{\Theta}) = \begin{bmatrix} m_T & 0 & 0 & 0 \\ 0 & A_1 & A_4 & A_5 \\ 0 & A_4 & A_2 & A_6 \\ 0 & A_5 & A_6 & A_3 \end{bmatrix} \tag{2.38}$$

$$\mathbf{V}\left(\boldsymbol{\Theta}, \dot{\boldsymbol{\Theta}}\right) = \begin{bmatrix} 0 \\ A_7 \\ A_8 \\ 0 \end{bmatrix} \tag{2.39}$$

$$\mathbf{G}(\boldsymbol{\Theta}) = \begin{bmatrix} -gm_T \\ 0 \\ 0 \\ 0 \end{bmatrix} \tag{2.40}$$

$$\boldsymbol{\Theta} = \begin{bmatrix} d_1 \\ \theta_1 \\ \theta_2 \\ \theta_3 \end{bmatrix} \tag{2.41}$$

$$\dot{\boldsymbol{\Theta}} = \begin{bmatrix} \dot{d}_1 \\ \dot{\theta}_1 \\ \dot{\theta}_2 \\ \dot{\theta}_3 \end{bmatrix} \tag{2.42}$$

$$\ddot{\boldsymbol{\Theta}} = \begin{bmatrix} \ddot{d}_1 \\ \ddot{\theta}_1 \\ \ddot{\theta}_2 \\ \ddot{\theta}_3 \end{bmatrix} \tag{2.43}$$

For the Sliding Mode Control, equation (2.3) is rewritten to have the form of

$$\boldsymbol{\tau} = \mathbf{M}(\boldsymbol{\Theta})\ddot{\boldsymbol{\Theta}} + \mathbf{Vn}\left(\boldsymbol{\Theta}, \dot{\boldsymbol{\Theta}}\right)\dot{\boldsymbol{\Theta}} + \mathbf{G}(\boldsymbol{\Theta}) \tag{2.44}$$

Where

$$\mathbf{Vn}\left(\boldsymbol{\Theta}, \dot{\boldsymbol{\Theta}}\right) = \begin{bmatrix} 0 & 0 & 0 & 0 \\ B_1 & B_2 & 0 & 0 \\ B_3 & 0 & 0 & 0 \\ 0 & 0 & 0 & 0 \end{bmatrix} \tag{2.45}$$

$$B_1 = -\left(m_3(a_2a_3s_2) + (2a_2a_3s_2)(m_4 + m_5)\right)\dot{\theta}_2 \tag{2.46}$$

$$B_2 = -(a_2 a_3 s_2)\left(\frac{1}{2}m_3 + m_4 + m_5\right)\dot{\theta}_2 \tag{2.47}$$

$$B_3 = = -\left(\frac{1}{2}m_3(a_2 a_3 s_2) + (a_2 a_3 s_2)(m_4 + m_5)\right)\dot{\theta}_2 \tag{2.48}$$

APPENDIX 3

A3-1 SMC DERIVATIVE

The Sliding Mode Control is derived as follows:

The first phase (reachability) uses the following gain:

$$\mathbf{u} = -\mathbf{M}(\boldsymbol{\Theta})\mathbf{K}\,sign(\mathbf{S}) \tag{3.1}$$

The second phase (sliding) has an equivalent control signal that is derived by setting $\dot{\mathbf{S}} = \mathbf{0}$ as follows:

$$\dot{\mathbf{S}} = \dot{\mathbf{e}} + \boldsymbol{\lambda}\ddot{\mathbf{e}} = \dot{\mathbf{e}} + \boldsymbol{\lambda}\left(\ddot{\boldsymbol{\Theta}} - \ddot{\boldsymbol{\Theta}}_d\right) = \dot{\mathbf{e}} + \boldsymbol{\lambda}\left(\mathbf{M}^{-1}(\boldsymbol{\Theta})\left(\boldsymbol{\tau} - \mathbf{Vn}\left(\boldsymbol{\Theta}, \dot{\boldsymbol{\Theta}}\right)\dot{\boldsymbol{\Theta}} - \mathbf{G}(\boldsymbol{\Theta})\right) - \ddot{\boldsymbol{\Theta}}_d\right) = \mathbf{0} \tag{3.2}$$

$$-\left(\boldsymbol{\lambda}\mathbf{M}^{-1}(\boldsymbol{\Theta})\right)^{-1}\dot{\mathbf{e}} + \left(\boldsymbol{\lambda}\mathbf{M}^{-1}(\boldsymbol{\Theta})\right)^{-1}\left(\boldsymbol{\lambda}\ddot{\boldsymbol{\Theta}}_d + \boldsymbol{\lambda}\mathbf{M}^{-1}(\boldsymbol{\Theta})\left(\mathbf{Vn}\left(\boldsymbol{\Theta}, \dot{\boldsymbol{\Theta}}\right)\dot{\boldsymbol{\Theta}} + \mathbf{G}(\boldsymbol{\Theta})\right)\right) = \mathbf{u}_{eq} \tag{3.3}$$

$$-\left(\boldsymbol{\lambda}\mathbf{M}^{-1}(\boldsymbol{\Theta})\right)^{-1}\dot{\mathbf{e}} + \left(\boldsymbol{\lambda}\mathbf{M}^{-1}(\boldsymbol{\Theta})\right)^{-1}\boldsymbol{\lambda}\ddot{\boldsymbol{\Theta}}_d + \mathbf{Vn}\left(\boldsymbol{\Theta}, \dot{\boldsymbol{\Theta}}\right)\dot{\boldsymbol{\Theta}} + \mathbf{G}(\boldsymbol{\Theta}) = \mathbf{u}_{eq} \tag{3.4}$$

$$-\mathbf{M}(\boldsymbol{\Theta})\boldsymbol{\lambda}^{-1}\dot{\mathbf{e}} + \mathbf{M}(\boldsymbol{\Theta})\ddot{\boldsymbol{\Theta}}_d + \mathbf{Vn}\left(\boldsymbol{\Theta}, \dot{\boldsymbol{\Theta}}\right)\dot{\boldsymbol{\Theta}} + \mathbf{G}(\boldsymbol{\Theta}) = \mathbf{u}_{eq} \tag{3.5}$$

$$\mathbf{u}_{eq} = \mathbf{M}(\boldsymbol{\Theta})\left(\ddot{\boldsymbol{\Theta}}_d - \boldsymbol{\lambda}^{-1}\left(\dot{\boldsymbol{\Theta}} - \dot{\boldsymbol{\Theta}}_{\mathbf{d}}\right)\right) + \mathbf{Vn}\left(\boldsymbol{\Theta}, \dot{\boldsymbol{\Theta}}\right)\dot{\boldsymbol{\Theta}} + \mathbf{G}(\boldsymbol{\Theta}) \tag{3.6}$$

Using $\mathbf{S} = \mathbf{e} + \boldsymbol{\lambda}\dot{\mathbf{e}} = \mathbf{0} \rightarrow \dot{\mathbf{e}} = -\boldsymbol{\lambda}^{-1}\mathbf{e} \rightarrow \dot{\boldsymbol{\Theta}} - \dot{\boldsymbol{\Theta}}_{\mathbf{d}} = -\boldsymbol{\lambda}^{-1}(\boldsymbol{\Theta} - \boldsymbol{\Theta}_{\mathbf{d}}) \rightarrow \dot{\boldsymbol{\Theta}} = \dot{\boldsymbol{\Theta}}_{\mathbf{d}} - \boldsymbol{\lambda}^{-1}(\boldsymbol{\Theta} - \boldsymbol{\Theta}_{\mathbf{d}})$ yields**:**

$$\mathbf{u}_{eq} = \mathbf{M}(\boldsymbol{\Theta})\left(\ddot{\boldsymbol{\Theta}}_d + \boldsymbol{\lambda}^{-1}\left(\dot{\boldsymbol{\Theta}} - \dot{\boldsymbol{\Theta}}_{\mathbf{d}}\right)\right) + \mathbf{Vn}\left(\boldsymbol{\Theta}, \dot{\boldsymbol{\Theta}}\right)\left(\dot{\boldsymbol{\Theta}}_d - \boldsymbol{\lambda}^{-1}(\boldsymbol{\Theta} - \boldsymbol{\Theta}_{\mathbf{d}})\right) + \mathbf{G}(\boldsymbol{\Theta}) \tag{3.7}$$

And $\boldsymbol{\tau}$**,** the total control signal, is defined as**:**

$$\boldsymbol{\tau} = -\mathbf{M}(\boldsymbol{\Theta})\mathbf{K}\,sign(\mathbf{S}) + \mathbf{M}(\boldsymbol{\Theta})\left(\ddot{\boldsymbol{\Theta}}_d + \boldsymbol{\lambda}^{-1}\left(\dot{\boldsymbol{\Theta}} - \dot{\boldsymbol{\Theta}}_{\mathbf{d}}\right)\right) + \mathbf{Vn}\left(\boldsymbol{\Theta}, \dot{\boldsymbol{\Theta}}\right)\left(\dot{\boldsymbol{\Theta}}_d - \boldsymbol{\lambda}^{-1}(\boldsymbol{\Theta} - \boldsymbol{\Theta}_{\mathbf{d}})\right) + \mathbf{G}(\boldsymbol{\Theta}) \tag{3.8}$$

A3-2 STABILITY OF OVERALL SYSTEM

Knowing that $\mathbf{z}, \mathbf{z}_{\mathbf{d}}$ and $\hat{\mathbf{z}}$ are the actual, desired and estimated system measurement vectors, respectively, and defining $\mathbf{e} = \mathbf{z} - \mathbf{z}_{\mathbf{d}}$, $\mathbf{e}_{\mathbf{c}} = \hat{\mathbf{z}} - \mathbf{z}_{\mathbf{d}}$, and $\hat{\mathbf{e}} = \hat{\mathbf{z}} - \mathbf{z}$, then the sliding surface for the SMC is defined as:

$$\mathbf{S} = \mathbf{e} + \boldsymbol{\lambda}\dot{\mathbf{e}} \tag{3.9}$$

If the Lyapunov function $\mathbf{V}$ is defined to be $\mathbf{V} = \frac{1}{2}\mathbf{S}\mathbf{S}^T > 0$, then $\dot{\mathbf{V}}$ is defined as**:**

$$\dot{\mathbf{V}} = \dot{\mathbf{S}}\mathbf{S}^T = (\dot{\mathbf{e}} + \boldsymbol{\lambda}\ddot{\mathbf{e}})(\mathbf{e} + \boldsymbol{\lambda}\dot{\mathbf{e}}\ )^{\boldsymbol{T}} \tag{3.10}$$

Where $\mathbf{e} + \boldsymbol{\lambda}\dot{\mathbf{e}}$ is defined as

$$\mathbf{e} + \boldsymbol{\lambda}\dot{\mathbf{e}} = \boldsymbol{H}\left(\boldsymbol{\Theta} - \boldsymbol{\Theta}_{\mathbf{d}} + \boldsymbol{\lambda}\left(\dot{\boldsymbol{\Theta}} - \dot{\boldsymbol{\Theta}}_{\mathbf{d}}\right)\right) \tag{3.11}$$

And $\dot{\mathbf{e}} + \boldsymbol{\lambda}\ddot{\mathbf{e}}$

$$\dot{\mathbf{e}} + \boldsymbol{\lambda}\ddot{\mathbf{e}} = \boldsymbol{H}\left(\dot{\boldsymbol{\Theta}} - \dot{\boldsymbol{\Theta}}_{\mathbf{d}} + \boldsymbol{\lambda}\left(\ddot{\boldsymbol{\Theta}} - \ddot{\boldsymbol{\Theta}}_{\mathbf{d}}\right)\right) \tag{3.12}$$

Substitute (3.2) in (3.12), then (3.13) is obtained as follows:

$$\dot{\mathbf{S}} = \dot{\mathbf{e}} + \boldsymbol{H\lambda}\left(\mathbf{M}^{-1}(\boldsymbol{\Theta})\left[\boldsymbol{\tau} - \mathbf{Vn}\left(\dot{\boldsymbol{\Theta}}, \dot{\boldsymbol{\Theta}}\right)\dot{\boldsymbol{\Theta}} - \mathbf{G}(\boldsymbol{\Theta})\right] - \ddot{\boldsymbol{\Theta}}_{d}\right) \tag{3.13}$$

$\boldsymbol{\tau}$ is defined by the estimated measurement vector as**:**

$$\boldsymbol{\tau} = -\mathbf{M}(\widehat{\boldsymbol{\Theta}})\mathbf{K}\, sign(\widehat{\mathbf{S}}) + \mathbf{M}(\widehat{\boldsymbol{\Theta}})\left(\ddot{\boldsymbol{\Theta}}_{d} - \boldsymbol{\lambda}^{-1}\left(\dot{\widehat{\boldsymbol{\Theta}}} - \dot{\boldsymbol{\Theta}}_{\mathbf{d}}\right)\right) + \mathbf{Vn}\left(\widehat{\boldsymbol{\Theta}}, \dot{\widehat{\boldsymbol{\Theta}}}\right)\left(\dot{\boldsymbol{\Theta}}_{d} - \boldsymbol{\lambda}^{-1}\left(\widehat{\boldsymbol{\Theta}} - \boldsymbol{\Theta}_{\mathbf{d}}\right)\right) + \mathbf{G}(\widehat{\boldsymbol{\Theta}}) \tag{3.14}$$

Substituting (3.14) in (3.13) and rearranging give:

$$\dot{\mathbf{S}} = \boldsymbol{H}\left(\dot{\boldsymbol{\Theta}} - \dot{\boldsymbol{\Theta}}_{\mathbf{d}}\right) + \boldsymbol{H\lambda}\left(\mathbf{M}^{-1}(\boldsymbol{\Theta})\left[\left\{\begin{array}{c} -\mathbf{M}(\widehat{\boldsymbol{\Theta}})\mathbf{K}\, sign(\widehat{\mathbf{S}}) \\ + \mathbf{M}(\widehat{\boldsymbol{\Theta}})\left(\ddot{\boldsymbol{\Theta}}_{d} - \boldsymbol{\lambda}^{-1}\left(\dot{\widehat{\boldsymbol{\Theta}}} - \dot{\boldsymbol{\Theta}}_{\mathbf{d}}\right)\right) - \mathbf{M}(\boldsymbol{\Theta})\ddot{\boldsymbol{\Theta}}_{d} \\ + \left[\mathbf{Vn}\left(\widehat{\boldsymbol{\Theta}}, \dot{\widehat{\boldsymbol{\Theta}}}\right)\dot{\widehat{\boldsymbol{\Theta}}} - \mathbf{Vn}\left(\dot{\boldsymbol{\Theta}}, \dot{\boldsymbol{\Theta}}\right)\dot{\boldsymbol{\Theta}}\right] \\ +\mathbf{G}(\widehat{\boldsymbol{\Theta}}) - \mathbf{G}(\boldsymbol{\Theta}) \end{array}\right\}\right]\right) \tag{3.15}$$

For simplicity, (3.15) becomes (3.16).

$$\dot{\mathbf{S}} = \boldsymbol{H\lambda}\mathbf{M}^{-1}(\boldsymbol{\Theta})\left[-\mathbf{M}(\widehat{\boldsymbol{\Theta}})\mathbf{K}\, sign(\widehat{\mathbf{S}}) + \left(\begin{array}{c} \mathbf{M}(\widehat{\boldsymbol{\Theta}})\ddot{\boldsymbol{\Theta}}_{d} - \mathbf{M}(\boldsymbol{\Theta})\ddot{\boldsymbol{\Theta}}_{d} \\ -\mathbf{M}(\widehat{\boldsymbol{\Theta}})\boldsymbol{\lambda}^{-1}\left(\dot{\widehat{\boldsymbol{\Theta}}} - \dot{\boldsymbol{\Theta}}_{\mathbf{d}}\right) + \mathbf{M}(\boldsymbol{\Theta})\boldsymbol{\lambda}^{-1}\left(\dot{\boldsymbol{\Theta}} - \dot{\boldsymbol{\Theta}}_{\mathbf{d}}\right) \\ + \left[\mathbf{Vn}\left(\widehat{\boldsymbol{\Theta}}, \dot{\widehat{\boldsymbol{\Theta}}}\right)\dot{\widehat{\boldsymbol{\Theta}}} - \mathbf{Vn}\left(\dot{\boldsymbol{\Theta}}, \dot{\boldsymbol{\Theta}}\right)\dot{\boldsymbol{\Theta}}\right] \\ +\mathbf{G}(\widehat{\boldsymbol{\Theta}}) - \mathbf{G}(\boldsymbol{\Theta}) \end{array}\right)\right] \tag{3.16}$$

Knowing that $\boldsymbol{H}, \boldsymbol{\lambda}$ and $\mathbf{M}^{-1}(\boldsymbol{\Theta})$ are positive matrices, and choosing $\mathbf{K}$ to be:

$$\boldsymbol{K} \geq \left\{\left|\boldsymbol{M}^{-1}(\widehat{\boldsymbol{\Theta}})\left(\begin{array}{c} \boldsymbol{M}(\widehat{\boldsymbol{\Theta}})\ddot{\boldsymbol{\Theta}}_{d} - \boldsymbol{M}(\boldsymbol{\Theta})\ddot{\boldsymbol{\Theta}}_{d} \\ +\boldsymbol{M}(\widehat{\boldsymbol{\Theta}})\boldsymbol{\lambda}^{-1}\left(\dot{\widehat{\boldsymbol{\Theta}}} - \dot{\boldsymbol{\Theta}}_{d}\right) + \boldsymbol{M}(\boldsymbol{\Theta})\boldsymbol{\lambda}^{-1}\dot{\boldsymbol{e}}\left(\dot{\boldsymbol{\Theta}} - \dot{\boldsymbol{\Theta}}_{d}\right) \\ + \left[\boldsymbol{Vn}\left(\widehat{\boldsymbol{\Theta}}, \dot{\widehat{\boldsymbol{\Theta}}}\right)\dot{\widehat{\boldsymbol{\Theta}}} - \boldsymbol{Vn}\left(\dot{\boldsymbol{\Theta}}, \dot{\boldsymbol{\Theta}}\right)\dot{\boldsymbol{\Theta}}\right] \\ +\boldsymbol{G}(\widehat{\boldsymbol{\Theta}}) - \boldsymbol{G}(\boldsymbol{\Theta}) \end{array}\right)\right|_{MAX}\right\} \tag{3.17}$$

Then $\dot{\mathbf{S}}$ will have the sign of $\left[-\mathbf{M}(\widehat{\boldsymbol{\Theta}})\mathbf{K}\, sign(\widehat{\mathbf{S}})\right]$, and $\dot{\mathbf{V}} = \dot{\mathbf{S}}\mathbf{S}^{T}$ becomes

$$\dot{\mathbf{V}} = -\boldsymbol{H\lambda}\mathbf{M}^{-1}(\boldsymbol{\Theta})\mathbf{M}(\widehat{\boldsymbol{\Theta}})\mathbf{K}sign(\widehat{\mathbf{S}})\mathbf{S}^{T} \tag{3.18}$$

The system is stable if

$$sign(\widehat{\mathbf{S}})\mathbf{S}^{T} \geq 0 \tag{3.19}$$

Which means that

$$\widehat{\boldsymbol{S}} \cong \boldsymbol{S} \textbf{ or } \widehat{\boldsymbol{\Theta}} \cong \boldsymbol{\Theta} \tag{3.20}$$

The proposed method is less sensitive to noise compared to conventional SVSF, and it is less sensitive to the covariance matrices compared to the older version of the UK-SVSF. This is why (3.20) is more achievable in the proposed method compared to the rest. Moreover, it needs less computational time compared to the last one.

Appendix 4

The derivation of the smooth boundary layer of the proposed method is as follows:

The cost function is defined by the following equation:

$$\mathrm{J} = \left(\mathbf{e}_{x,2_{k|k}}\mathbf{e}_{x,2_{k|k}}^{T}\right) = \left(\mathbf{e}_{z,2_{k|k}} - \mathbf{v}_k\right)\left(\mathbf{e}_{z,2_{k|k}} - \mathbf{v}_k\right)^{T} \tag{4.1}$$

Where $\mathbf{e}_{z,2_{k|k}}$ is the a priori measurement estimation error for the second filter and is defined as:

$$\mathbf{e}_{z,2_{k|k}} = \mathbf{e}_{z,2_{k|k-1}} - \mathbf{H}\mathbf{K}_{SVSF} = \mathbf{e}_{z,2_{k|k-1}} - \left(\left|\mathbf{e}_{z,2_{k|k-1}}\right| + \boldsymbol{\gamma}\left|\mathbf{e}_{z,2_{k-1|k-1}}\right|\right)\circ \boldsymbol{sat}\left(\frac{\mathbf{e}_{z,1_{k|k-1}}}{\boldsymbol{\Psi}_{\mathrm{tv_k}}}\right) \tag{4.2}$$

Without losing generality, and for simplicity, assume $\mathbf{e}_{z,2_{k|k-1}} = \mathbf{e}_{z,1_{k|k-1}}$ (they have the same a posteriori estimates), $\mathbf{S}_{at} = \mathrm{diag}\left(\frac{\left|\mathrm{e}_{z,1_{k|k-1}}\right|}{\boldsymbol{\Psi}_{\mathrm{tv_k}}}\right)$ and $\boldsymbol{\gamma} = \mathbf{0}$ yields

$$\mathbf{e}_{z,2_{k|k}} = \mathbf{e}_{z,1_{k|k-1}} - \left(\left|\mathbf{e}_{z,1_{k|k-1}}\right|\right)\mathbf{S}_{at}\circ \boldsymbol{sign}\left(\mathbf{e}_{z,1_{k|k-1}}\right) = \mathbf{e}_{z,1_{k|k-1}} - \mathbf{S}_{at}\mathbf{e}_{z,1_{k|k-1}} \tag{4.3}$$

Substitute equation (4.3) in equation (4.1) gives:

$$\mathrm{J} = \left(\mathbf{e}_{z,1_{k|k-1}} - \mathbf{S}_{at}\mathbf{e}_{z,1_{k|k-1}} - \mathbf{v}_k\right)\left(\mathbf{e}_{z,1_{k|k-1}} - \mathbf{S}_{at}\mathbf{e}_{z,1_{k|k-1}} - \mathbf{v}_k\right)^{T} \tag{4.4}$$

Equation (4.4) is simplified to the following (after taking the expectation value and rearrange the terms):

$$\mathrm{J} = \mathrm{E}\left(\left(\mathbf{I}_{nxn} - \mathbf{S}_{at}\right)\mathbf{e}_{z,1_{k|k-1}} - \mathbf{v}_k\right)\left(\left(\mathbf{I}_{nxn} - \mathbf{S}_{at}\right)\mathbf{e}_{z,1_{k|k-1}} - \mathbf{v}_k\right)^{T} \tag{4.5}$$

$$\mathrm{J} = \mathrm{E}\left(\mathrm{diag}\left(\left(\mathbf{I}_{nxn} - \mathbf{S}_{at}\right)^{2}\mathbf{e}_{z,1_{k|k-1}}\mathbf{e}_{z,1_{k|k-1}}^{\mathbf{T}} - \left(\mathbf{I}_{nxn} - \mathbf{S}_{at}\right)\mathbf{v}_k\mathbf{e}_{z,1_{k|k-1}}^{\mathbf{T}} - \left(\mathbf{I}_{nxn} - \mathbf{S}_{at}\right)\mathbf{e}_{z,1_{k|k-1}}\mathbf{v}_k^{\mathbf{T}} + \mathbf{v}_k\mathbf{v}_k^{\mathbf{T}}\right)\right) \tag{4.6}$$

$$\mathrm{J} = \mathrm{diag}\left(\left(\mathbf{I}_{nxn} - \mathbf{S}_{at}\right)^{2}\mathbf{P}_{z,1_{k|k-1}} - 2\left(\mathbf{I}_{nxn} - \mathbf{S}_{at}\right)\mathbf{R}_k + \mathbf{R}_k\right) \tag{4.7}$$

Taking the derivative of J with respect to $\mathbf{S}_{at}$ yields:

$$\frac{\partial \mathrm{J}}{\partial \mathbf{S}_{at}} = \mathrm{diag}\left(-2\left(\mathbf{I}_{nxn} - \mathbf{S}_{at}\right)\mathbf{P}_{z,1_{k|k-1}} + 2\mathbf{R}_k\right) = 0 \tag{4.8}$$

$$\mathbf{S}_{at} = diag\left(\frac{\mathbf{e}_{z,1_{k|k-1}}}{\boldsymbol{\Psi}_{\mathrm{tv_k}}}\right) = \left(\mathbf{P}_{zz_{1,k|k-1}} - \mathbf{R}_k\right)\circ \mathbf{I}_{nxn}\left(\left(\mathbf{P}_{zz_{1,k|k-1}}\circ \mathbf{I}_{nxn}\right)\right)^{-1} \tag{4.9}$$

$$\boldsymbol{\Psi}_{\mathrm{tv_k}} = \left(\mathbf{P}_{zz_{1,k|k-1}}\circ \mathbf{I}_{nxn}\right)\left(\left(\mathbf{P}_{zz_{1,k|k-1}} - \mathbf{R}_k\right)\circ \mathbf{I}_{nxn}\right)^{-1}\left|\mathbf{e}_{z,1_{k|k-1}}\right| \tag{4.10}$$

REFERENCES

[1] Salehi, A., Piltan, F., Mirshekaran, M., Kazeminasab, M. and Esmaeili, Z., 2014, “Comparative Study between Two Important Nonlinear Methodologies for Continuum Robot Manipulator Control” I.J. Information Technology and Computer Science, 6(4), pp. 66-80.
[2] Mondragon, C., Fotouhi, R., 2012, “Dynamics and Motion Control of a 6-DOF Robot Manipulator” ASME 2012 International Mechanical Engineering Congress and Exposition. Houston, TX, Vol. 4, pp. 369-380.
[3] Soltani, S., Piltan, F., 2011, “Design Artificial Nonlinear Controller Based on Computed Torque like Controller with Tunable Gain”. World Applied Science Journal, 14(9), pp. 1306-1312.
[4] Piltan, F., Haghighi, S., Sulaima, N., Nazari, I., Siamak, S., 2011, “Artificial Control of PUMA Robot Manipulator: A-Review of Fuzzy Inference Engine and Application to Classical controller” International Journal of Robotic and Automation (IJRA), 2(5), pp.401-425.
[5] Horspool, K., 2003, Cartesian-space Adaptive Control for Dual-arm Force Control Using Industrial Robots. University of New Mexico.
[6] Ashrafiuon, H., Reddy, J. V., 2005, “Model-Based Sliding Mode Control for a Robot with SMA Actuators” ASME 2005 International Design Engineering Technical Conferences and Computers and Information in Engineering Conference. Vol. 7: 29th Mechanisms and Robotics Conference, Parts A and B, Long Beach, California, pp. 615-621.
[7] Piltan, F., Mehrara, S., Bayat, R., Rahmdel, S., 2012 “Design New Control Methodology of Industrial Robot Manipulator: Sliding Mode Baseline Methodology.” International Journal of Hybrid Information Technology. 5(4), pp. 41-54.
[8] Piltan, F., Gavahian, A., Sulaiman, N., Marhaban, M.H., 2011 “Novel Sliding Mode Controller for Robot Manipulator using FPGA” Journal of Advanced Science and Engineering Research. 1(1) ,pp. 1-22.
[9] Kailath, T., 1974, “A View of Three Decades Of Linear Filtering Theory”, IEEE Transactions on Information Theory, IT-20(2), pp. 146-181.
[10] Trafina, T., 2018, “Kalman filter application for localization improvement of multi-copter UAV”, Master’s Project, Faculty of Electrical Engineering, Department of Computer Science, Czech Technical University in Prague.
[11] Simon, D, 2006, “Optimal State Estimation: Kalman, H [infinity] And Nonlinear Approaches”, Wiley-Interscience.
[12] Bar-Shalom, T., Li, X., and Kirubarajan, T., 2001, “Estimation with Applications to Tracking and Navigation – Theory, Algorithm and Software”, John Wiley & Sons, Inc.
[13] Kim, D., and Park, C., 2017, “Application of Kalman Filter for Estimating a Process Disturbance in a Building Space”, Sustainability, Vol. 9, Issue 10, 1868.
[14] Grewal, M., and Andrews, A., 2001, “Kalman Filtering: Theory and Practice Using Matlab”, Second Edition, John Wiley & Sons Inc., USA.
[15] Mahhoub, V., and Mohammadi, D., 2018, “A Constrained Total Extended Kalman Filter for Integrated Navigation”, The Journal of Navigation, Vol. 71, Issue 4, pp. 971-988.
[16] Oh, K., Song, T., and Lee, H., 2018, “An Extended Kalman Filter Based Object Tracking Algorithm for Autonomous Guided Truck Using 1-Layer Laser Scanner”, ASME-JSME 2018 Joint International Conference on Information Storage and Processing Systems and Micromechatronics for Information and Precision Equipment San Francisco, California, USA, August 29–30, 2018.
[17] Xiong, K., and Wei, C., 2017, “Adaptive Iterated Extended KALMAN Filter for Relative Spacecraft Attitude and Position Estimation”, Asian Journal of Control, Vol 20, Issue 4, pp. 1595-1610.
[18] Hu, X., Bao, M., Zhang, X., Guan, L., and Hu, Y., 2015, "Generalized Iterated Kalman Filter and its Performance Evaluation," IEEE Transactions on Signal Processing, Vol. 63, no. 12, pp. 3204-3217.
[19 García-Pintado, J., and Paul, A., 2018, “Evaluation of iterative Kalman smoother schemes for multi-decadal past climate analysis with comprehensive Earth system models”, Geoscientific Model Development, Vol. 11, pp. 5051–5084.
[20] Berber, S., Hirani, G., and Ho, M., 2014, “Measurement and Mean Power Estimation in Indoor Wireless Channel Based on Higher Order Kalman Filtering”, IEEE Transactions on Instrumentation and Measurement Vol.

63, Issue 12, pp. 2771 - 2778.
[21] Fahimi, F., Kotike, S., and Rameshbabu, R., 2018, "A Self-Levelling Higher Order Sliding Mode Controller For A Leg-Wheeled Robot With Experiments." Mechatronic Systems and Control, Vol. 46, Issue 3.
[22] Nguyen, N., Yang, H., and Kim, S., 2017, "HOKF: High Order Kalman Filter for Epilepsy Forecasting Modeling", Biosystems, Vol. 158, pp. 57-67.
[23] Van Der Heidan, F., Duin, R., de Ridder, D., and Tax, C., 2004, "Classification, Parameter Estimation and State Estimation – An Engineering Approach Using MATLAB", John Wiley & Sons, Ltd., England.
[24] Duník, J., Straka, O., Šimandl, O., & Blash, E. (2016). Sigma-Point Set Rotation for Derivative-Free Filters in Target Tracking Applications. Journal of Advances in Information Fusion, 11(1), 91 - 109.
[25] Ritter, B., Mora, E., Schlicht, T., Schild, A., and Konigorski, U., 2018, "Adaptive Sigma-Point Kalman Filtering for Wind Turbine State and Process Noise Estimation", Journal of Physics: Conference Series, Published under licence by IOP Publishing Ltd, Volume 1037.
[26] Liu, G., and Tian, G., 2017, "Square-Root Sigma-Point Information Consensus Filters for Distributed Nonlinear Estimation", Sensors (Basel), Vol. 17, Issue 4.
[27]Yan, H., Gao, B., Gao, S., Xue, L., Zhong, Y., Gu, C., and Jazar, R., 2016, "Robust Adaptive Gaussian Mixture Sigma Point Particle Filter", Journal of Robotics and Automation, Vol. 1, Issue 1, pp. 1-7.
[28] Martin, A., and Emami, M., 2014, "Just-In-Time Cooperative Simultaneous Localization And Mapping: A Robust Particle Filter Approach." International Journal of Robotics and Automation, Vol. 29, Issue 2.
[29] Al-Saggaf, U., Bettayeb, M., and Djennoune, S., 2017, "Super-Twisting Algorithm-Based Sliding-Mode Observer for Synchronization of Nonlinear Incommensurate Fractional-Order Chaotic Systems Subject to Unknown Inputs", Arabian Journal for Science and Engineering, pp. 3065 - 3075, 42(7).
[30] Zhao, K., Zhang, C., Li, X., He, J., and Lin, Y., 2017, "Sliding Mode Observer-Based Current Sensor Fault Reconstruction and Unknown Load Disturbance Estimation for PMSM Driven System", Sensors, MDPI, 17(12).
[31] Li, R., and Zhang, Q., 2018. "Robust H∞ sliding mode observer design for a class of Takagi–Sugeno fuzzy descriptor systems with time-varying delay," Applied Mathematics and Computation, Elsevier, vol. 337(C), pages 158-178.
[32] Le, Q., Kang, H., and Le, T., 2018, "An Adaptive Controller with An Orthogonal Neural Network and A Third Order Sliding Mode Observer for Robot Manipulators", International Journal of Mechanical Engineering and Robotics Research, 7(2), pp. 169-173.
[33] Venkatesan, M., and Ravi, V., 2014, "Sliding mode observer based sliding mode controller for interacting nonlinear system", Second International Conference on Current Trends In Engineering and Technology - ICCTET 2014, IEEE, India.
[34] Yue, C. and Chen, H., 2018, "Adaptive Sliding-Mode Tracking Control for an Uncertain Nonlinear SISO Servo System with a Disturbance Observer", Journal of Shanghai Jiaotong University (Science), Vol. 23, Issue 2, pp. 376-383.
[35] Chawengkrittayanont, P., Pukdeboon, C., 2018, "Continuous higher order sliding mode observers for a class of uncertain nonlinear systems." Transactions of the Institute of Measurement and Control, DOI: 10.1177/0142331218769130.
[36] He, J., Mi, L., Liu, J., Cheng, X., Lin, Z., and Zhang, C., 2018, "Ring Coupling-Based Collaborative Fault-Tolerant Control For Multi-Robot Actuator Fault." International Journal of Robotics and Automation, 33(6).
[37] Chu, Z., Zhu, D. and Yang, X., 2016, "Adaptive Terminal Sliding Mode Based Sensorless Speed Control For Underwater Thruster." International Journal of Robotics and Automation, 31(3).
[38] H. H. Afshari, S. A. Gadsden, and S. R. Habibi, 2014, "Robust Fault Diagnosis of an Electrohydrostatic Actuator using the Novel Optimal Second-Order SVSF and IMM Strategy", International Journal of Fluid Power, 15(3), p.p. 181 – 196.
[39] S. A. Gadsden, 2011, "Smooth Variable Structure Filtering: Theory and Applications", PhD Thesis, Hamilton, Ontario, Canada.
[40] S. A. Gadsden and A. S. Lee, 2017, "Advances of the Smooth Variable Structure Filter: Square-Root and Two-Pass Formulations", Journal of Applied Remote Sensing, 11(1).
[41] H. H. Afshari, S. A. Gadsden, and S. R. Habibi, 2017, "Gaussian Filters for Parameter and State Estimation: A

General Review and Recent Trends", Signal Processing, 135, p. p. 218-238.
[42] S. A. Gadsden, S. R. Habibi, and T. Kirubarajan, 2014, "Kalman and Smooth Variable Structure Filters for Robust Estimation", IEEE Transactions on Aerospace and Electronic Systems, 50(2), p. p. 1038 – 1050.
[43] S. A. Gadsden and S. R. Habibi, 2013, "Novel Model-Based Estimators for the Purposes of Fault Detection and Diagnosis", IEEE/ASME Transactions on Mechatronics, 18(4), p. p. 1237 – 1249.
[44] S. A. Gadsden and S. R. Habibi, 2013, "A New Robust Filtering Strategy for Linear Systems", ASME Journal of Dynamic Systems, Measurement, and Control, 135(1).
[45] J. Goodman, J. Kim, A. S. Lee, S. A. Gadsden, and M. Al-Shabi, "A Variable Structure-Based Estimation Strategy Applied to an RRR Robot System", Journal of Robotics, Networking, and Artificial Life, 4(2), p. p. 142 – 145.
[46] S. A. Gadsden, M. Al-Shabi, and S. R. Habibi, 2011, "Estimation Strategies for the Condition Monitoring of a Battery System in a Hybrid Electric Vehicle", ISRN Signal Processing.
[47] S. A. Gadsden, M. Al-Shabi, I. Arasaratnam, and S. R. Habibi, 2010, "Estimation of an Electrohydrostatic Actuator Using a Combined Cubature Kalman and Smooth Variable Structure Filter", International Mechanical Engineering Congress and Exposition (IMECE), American Society of Mechanical Engineers, Vancouver, British Columbia.
[48] M. Al-Shabi, A. Cataford, and S. A. Gadsden, "Quadrature Kalman Filters with Applications to Robotic Manipulators", 2017 IEEE International Symposium on Robotics and Intelligent Sensors, Ottawa, Ontario.
[49] M. Al-Shabi and S. R. Habibi, 2013, "New Novel Time-Varying, Stable and Robust Smoothing Boundary Layer Width for the Smooth Variable Structure Filter", International Symposium on Mechatronics and its Applications (ISMA'13), Amman-Jordan.
[50] S. A. Gadsden, M. Al-Shabi, I. Arasaratnam, and S. R. Habibi, 2014, "Combined Cubature Kalman and Smooth Variable Structure Filtering: A Robust Nonlinear Estimation Strategy", Signal Processing, 96(B), p. p. 290 – 299.
[51] M. Alshabi, K. Hatamleh, S. AlShaer, I. Salameh, and S. A. Gadsden, "A Comprehensive Comparison of Sigma-Point Kalman Filters applied on a Complex Maneuvering Road", 2016 SPIE Signal Processing, Sensor/Information Fusion, and Target Recognition XXV, Baltimore, Maryland.
[52] J. Craig, 2005, Introduction to Robotics Mechanics and Control. Pearson Prentice Hall, Upper Saddle River, NJ.
[53] M. Al-Shabi and K. Hatamleh, "The Unscented Smooth Variable Structure Filter Application Into a Robotic Arm", ASME 2014 International Mechanical Engineering Congress and Exposition, Volume 4B: Dynamics, Vibration, and Control, Montreal, Quebec, Canada, November 14–20, 2014.
[54] Hatamleh, K., Al-Shabi, M., Khasawneh, Q. and Abo Al-Asal, M., "Application of SMC and NLFC Into a PRRR Robotic Arm", ASME 2014 International Mechanical Engineering Congress and Exposition, Volume 4A: Dynamics, Vibration, and Control, Montreal, Quebec, Canada, November 14–20, 2014.
[55] Al-Shabi, M., Bani-Yonis, M., and Hatamleh, K., "The sigma-point central difference smooth variable structure filter application into a robotic arm", 12th International Multi-Conference on Systems, Signals & Devices (SSD), Mahdia, Tunisia, 07 December 2015.
[56] Al-Shabi, M., "Sigma-Point Filters in Robotic Applications", Intelligent Control and Automation, 2015, 6, 168-183.
[57] Al-Shabi, M., "Sigma-point Smooth Variable Structure Filters applications into robotic arm", 7th International Conference on Modeling, Simulation, and Applied Optimization (ICMSAO), Sharjah, United Arab Emirates, 4-6 April 2017.
[58] Utkin, V., Guldner, J., Shi, J., 1999. Sliding Mode Control in Electromechanical Systems. Taylor & Francis Inc Philadelphia, PA.
[59] Ansari, U., and Bajodah, A., 2018. "Adaptive Fuzzy Sliding Mode Control: Application to Satellite Launch Vehicle's Attitude Control." Mechatronic Systems and Control, Vol. 46, Issue 1.
[60] Zhang, W., Liang, Z., Sun, X., Teng, Y., Song, X., and Yan, Z., 2017, "Path Following Control For An Under-Actuated UUV Based On Adaptive Sliding Mode Control." International Journal of Robotics and Automation, Vol. 32, Issue 5.
[61] Zhu, S., Chen, Q., Wang, X., and Liu, S., 2016, "Dynamic Modelling Using Screw Theory and Nonlinear Sliding Mode Control Of Serial Robot." International Journal of Robotics and Automation, Vol. 31, Issue 1.
[62] Perruquetti, W., Barbot, J., 2002. Sliding Mode Control In Engineering. Marcel Dekker, Inc, New York, NY.

[63] Al-Shabi, M., 2011, "The General Toeplitz/Observability Smooth Variable Structure Filter", PhD Thesis Dissertation, McMaster University.
[64] Al-Shabi M. and Habibi S., 2013, "New Novel time-varying, stable and Robust Smoothing Boundary Layer Width for the Smooth Variable Structure Filter", International Symposium on Mechatronics and its Applications (ISMA'13), Amman-Jordan.
[65] M. Al-Shabi and S. A. Gadsden, 2013, "Kalman Filtering Strategies Utilizing the Chattering Effects of the Smooth Variable Structure Filter", Signal Processing, 93(2), p. p. 420 – 4311.
[66] S. A. Gadsden and S. R. Habibi, 2010, "A new form of the smooth variable structure filter with a covariance derivation", 49th IEEE Conference on Decision and Control (CDC), p.p. 7389-7394.
[67] S. A. Gadsden, M. El Sayed, and S. R. Habibi, "Derivation of an Optimal Boundary Layer Width for the Smooth Variable Structure Filter", 2011 ASME/IEEE American Control Conference (ACC), San Francisco, California.